Journal of African Earth Sciences 174 (2021) 104013

Contents lists available at ScienceDirect

Journal of African Earth Sciences

journal homepage: www.elsevier.com/locate/jafrearsci

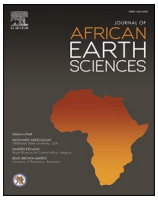

# Late Jurassic and Early Cretaceous sedimentation in the Mandawa Basin, coastal Tanzania

Katrine Fossum [a,*], Henning Dypvik [a], Muna H.M. Haid [a], Wellington E. Hudson [b], Majkel van den Brink [a]

[a] Department of Geosciences, University in Oslo, Boks 1047 Blindern, 0316 Oslo, Norway
[b] Tanzania Petroleum Development Corporation, P.O. Box 2774, Dar es Salaam, Tanzania

A B S T R A C T

This paper concerns the sedimentary successions deposited in the Mandawa Basin after the separation of East and West Gondwana during the subsequent southwards drift of Madagascar in the Late Jurassic to Early Cretaceous times. The aim of this study was to provide more specific details on the Late Jurassic and Early Cretaceous sedimentation and to report mineralogical and petrographical characteristics on the less well documented successions, namely the Kipatimu, Mitole and Nalwehe formations, in the central and northern parts of the Mandawa Basin.

The Late Jurassic and Early Cretaceous depositional environments are reviewed, based on the sedimentological, mineralogical and petrographical results presented here, supplemented by previously published work. The Late Jurassic to Early Cretaceous depositional setting mainly reflects a shallow, tidally influenced, mixed carbonate-silisiclastic coastal ramp. The succession displays cyclical sedimentation best described as a series of transgressive-regressive sequences with limestones overlain by siliciclastics. During transgressions microbial activity was high and sedimentation rates low, resulting in micro-oncoid deposition in the late Kimmeridgian – early Tithonian (Mitole Limestone Member), and oncoids and stromatolites in the Early Cretaceous (Nalwehe Limestone Member). During the regressive phases siliciclastic marginal marine sediments were deposited over the limestones. The regressive sandstones are mainly unfossiliferous and display evidence of being deposited in a tide-dominated, marginal marine environment.

## 1. Introduction

The Mandawa Basin of southern coastal Tanzania covers an area of c. 15,000 km$^2$ and is demarcated from the Rufiji Trough in the north by the E-W Utete-Tagalala Lineament, while the Ruvuma Saddle forms the southern border to the adjacent Ruvuma Basin (Fig. 1). The basin is separated from the Masasi Spur metamorphic basement in the west by a major NW-SE trending border fault following the Lindi trend (Figs. 1 and 2). In the east, the Mandawa Basin passes laterally into the offshore basins of the western Indian Ocean (Hudson, 2011).

The Late Jurassic to Early Cretaceous sedimentary evolution of the Mandawa Basin is the main focus of this paper. The Upper Jurassic and Lower Cretaceous formations have so far not been adequately documented with regards to sedimentology and their compositional characteristics. This paper aims to bring forward new sediment-petrographical data on the early post-rift successions in the Mandawa Basin by presenting detailed sedimentary logs and the mineralogical and petrographical characteristics of the studied formations.

Fieldwork was focused mainly on the less well documented successions, namely the Kipatimu, Mitole and Nalwehe formations, in the central and northern parts of the Mandawa Basin. This paper first presents the data and interpretations of recent investigations in the central area of the Mandawa Basin, and then those relating to the northern area (Fig. 2). A chronostratigraphic correlation was attempted between the Kipatimu Formation in the northern area and the Upper Jurassic and Lower Cretaceous successions in the central area. The last part of this paper is a synthesis of the proposed Late Jurassic to Early Cretaceous depositional environment, based on the results obtained by this study and available literature.

### 1.1. Regional geological background

The rifting which resulted in the separation of East and West Gondwana and the initiation of the Mandawa Basin commenced around 183–177 Ma (Geiger et al., 2004; Gaina et al., 2013; Reeves, 2018; Tuck-Martin et al., 2018). Extension occurred in a NW-SE direction in the newly opened Western Somali and Mozambique basins, and by dextral transtension along the margin segment between the two basins (Tuck-Martin et al., 2018). The rift to drift transition occurred around 170 Ma when Gondwana split roughly parallel to the modern East

* Corresponding author.
*E-mail address:* fossum.katrine@gmail.com (K. Fossum).

https://doi.org/10.1016/j.jafrearsci.2020.104013
Received 30 May 2019; Received in revised form 14 September 2020; Accepted 17 September 2020
Available online 25 September 2020

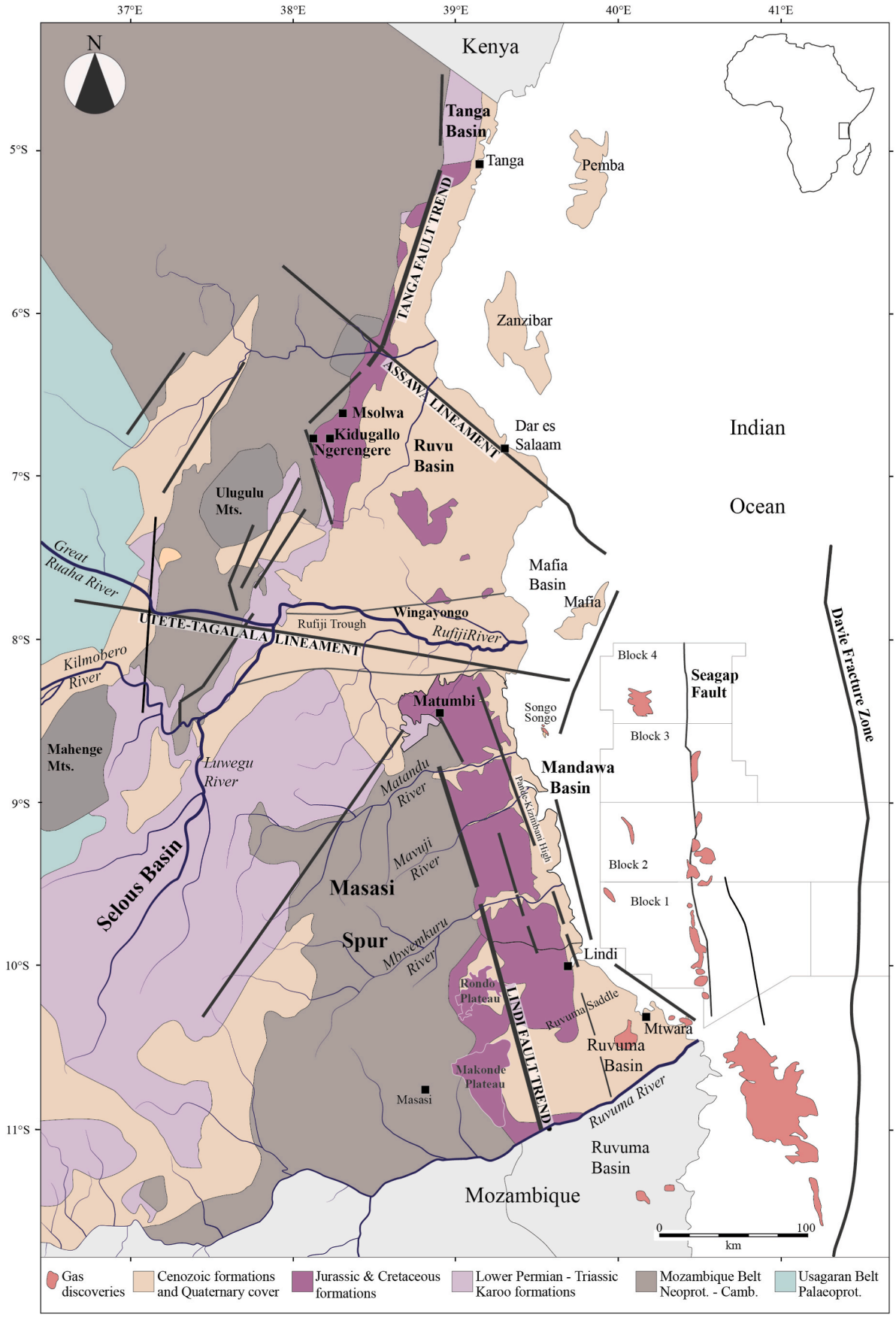


**Fig. 1.** Simplified geological map of Eastern Tanzania with the major tectonic lineaments and gas discoveries marked (Fossum, 2020).

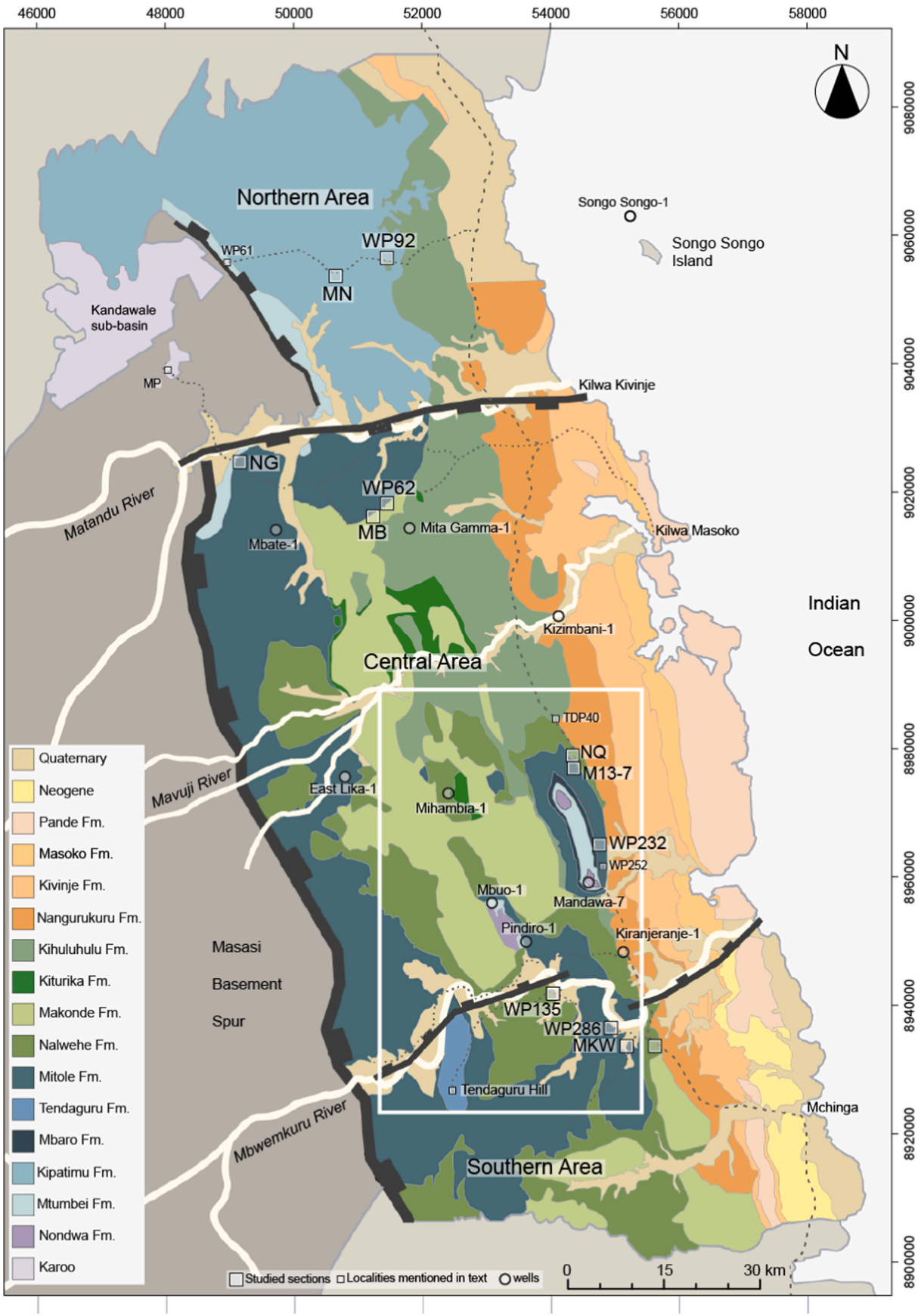


**Fig. 2.** Geological map of the Mandawa Basin. For the purpose of this paper the basin has been divided into three areas: northern, central and southern areas. Most of the geological investigations have been conducted in the central area. Modified from Fossum et al. (2018).

African Margin to form West Gondwana (South America and Africa) and East Gondwana (Madagascar, India, Australia and Antarctica) (Geiger et al., 2004; Gaina et al., 2013; Reeves, 2018). Seafloor spreading commenced shortly after in the Western Somali and Mozambique basins. The Seagap Fault (Fig. 1) probably originated as a dextral transform active during the early stages of seafloor spreading (Sansom, 2018). From about 140 Ma, pure dextral strike-slip motion was initiated along the 1800 km long Davie Fracture Zone (DFZ) (Gaina et al., 2013; Reeves, 2018).

In the early Aptian, the seafloor spreading in the Western Somali Basin and the transform movement along the DFZ ceased. A short-lived period of tectonic uplift followed the final movement along the DFZ (Mahanjane, 2014) which created a major unconformity along the margin segments bordering the Somali Basin in the end Hauterivian – Early Barremian (Tuck-Martin et al., 2018).

The plate boundary relocated south of Madagascar, eventually resulting in the breakup Madagascar/India and Antarctica. Dextral strike-slip motion was initiated between Madagascar and India in the Barremian (Gaina et al., 2013; Reeves, 2018; Tuck-Martin et al., 2018). After the separation of India and Madagascar in the Late Cretaceous, Madagascar was incorporated in the African Plate and a prolonged period of tectonic quiescence characterised the established East African Margin which lasted into the Miocene (Reeves, 2018).

### 1.2. *Upper Jurassic and Lower Cretaceous stratigraphy of the Mandawa Basin*

As no formal stratigraphic nomenclature exists for the Mandawa Basin, this study adapted the stratigraphic terminology of Hudson (2011).

During the Late Jurassic and Early Cretaceous the Mandawa Basin was part of a NE-dipping continental to shallow-marine ramp with mixed carbonate-siliciclastic sedimentation (Bussert and Aberhan, 2004). The cyclic character of the sedimentary infill (carbonates overlain by sandstones) partly suggests sediment deposition controlled by changes in relative sea-level. Sea-level fluctuations during this period were probably influenced by the opening of the Indian Ocean and the relative movement of India-Madagascar along the DFZ. Local tectonics include differences in subsidence rates and halokinesis that lasted until the Aptian (Didas, 2016). Several known or postulated unconformities in the Jurassic – Cretaceous sequence have been tied to salt diapiric movement and associated faulting (Aitken, 1961; Hudson, 2011).

#### 1.2.1. *Central mandawa area*

*1.2.1.1. Upper Jurassic.* The Upper Jurassic successions south of the Matandu River (Fig. 2) consist of alternating sequences of continental and marine units deposited during repeated sea-level fluctuations. During Oxfordian – middle Kimmeridgian times the central Mandawa Basin was a site for lagoonal and associated tidal flat sedimentation, which resulted in the deposition of the Mbaro Formation (Figs. 2 and 3) (Hudson, 2011).

The Tendaguru Hill area in southwestern Mandawa (Figs. 2 and 4) represents the most researched part of the Mandawa Basin, due to several dinosaur excavations conducted in the early 1900s (Bussert et al., 2009). The Late Jurassic deposition at Tendaguru was mainly marginal marine. This comprised lagoon-like, shallow marine embayments with widespread tidal flats and low-relief coastal plains (Aberhan et al., 2002). The Upper Jurassic to Lower Cretaceous Tendaguru Formation was formally described by Bussert et al. (2009), who subdivided the alternating marine and continental successions into six members (Fig. 4). The continental facies (Lower, Middle and Upper Dinosaur Members) include tidal flat, lagoonal and sabkha environments and are rich in fossil bones of sauropods and other dinosaurs. The dinosaur members are separated from each other by marine-dominated strata

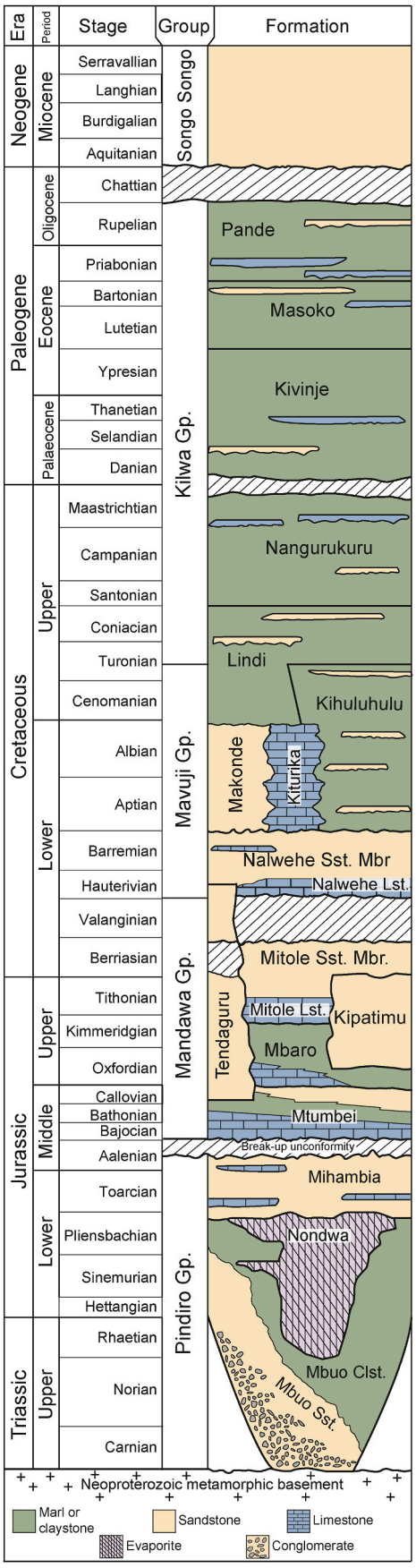


**Fig. 3.** Mandawa Basin stratigraphy, modified from Fossum et al. (2018).

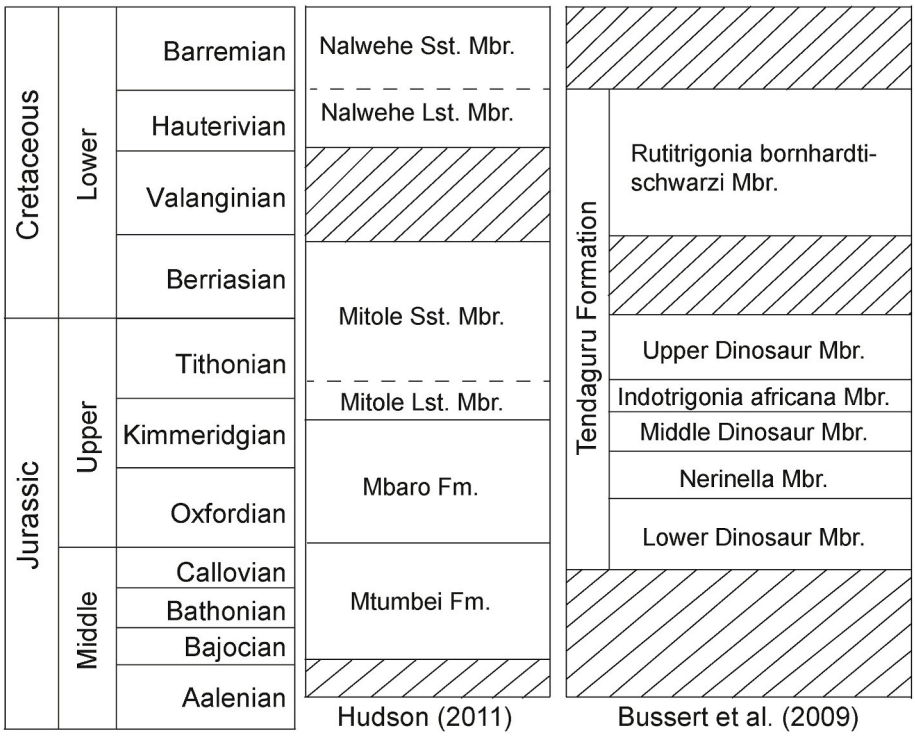


**Fig. 4.** Correlation of Tendaguru Formation with other formations in the Mandawa Basin. Compiled from Bussert et al. (2009) and Hudson (2011).

(such as tidal channels, sandbars and beach deposits), which are rich in marine fauna (Aberhan et al., 2002; Bussert et al., 2009). The Tendaguru area was generally tide-dominated, and sea-level fluctuations were an important factor controlling the sedimentation. Strict correlation of the Tendagruru Formation to other Upper Jurassic formations in the Mandawa Basin is challenging due to local unconformities and rapid shifts of lateral facies (Aitken, 1961).

The Mitole Formation (Figs. 2–5) comprises two members: a basal Limestone Member (late Kimmeridgian – early Tithonian) and an upper Sandstone Member (Tithonian – ?Berriasian) (Hudson, 2011). The Mitole Limestone Member is described as oolitic limestones (Hudson, 2011). In older literature the oolitic sequence of the Mitole Limestone Member was recognised as the "*smeei* Oolite" of Hennig (1914, in Quennel et al., 1956). The "*smeei* Oolite" occurs as discrete bands of coarse grained, well-bedded oolitic limestones intercalated with siliciclastic sandstones and non-oolitic limestones (e.g. Quennel et al., 1956; Aitken, 1961). The development of oolitic limestones is not consistent, but regarded as a regular feature of Upper Kimmeridgian – Tithonian strata in the south central parts of the Mandawa Basin (Aitken, 1961).

The Mitole Limestone Member is best exposed in the central area of the Mandawa Basin (Figs. 2 and 5). The oolitic limestones found encircling the Mandawa Dome (Fig. 5) occur in discrete bands interbedded with siltstones and yellow sandstones, and the interval in which ooids occur was estimated to be at least 106 m thick (Aitken, 1956). The eastern flank of the dome was considered the type area for the "*smeei* Oolite" (Quennel et al., 1956), and proposed as type section of the Mitole Limestone Member (Hudson, 2011). In the Mbwemkuru River depression and in the Pidiro Dome area, the oolitic limestones are found interbedded with calcareous sandstones (Aitken, 1955, 1961). In the Tendaguru area oolitic limestones have been reported to interfinger with the time-equivalent Indotrigonia Africana Member (Aitken, 1961; Aberhan et al., 2002; Bussert and Aberhan, 2004). The Indotrigonia Africana Member (Fig. 4) is about 30 m thick and consists of shallow marine sandstones (tidal channel sandstones, shell beds and sand bar deposits) deposited above fair-weather wave base (Aberhan et al., 2002; Bussert et al., 2009).

The overlying Mitole Sandstone Member was deposited during a regressive phase and comprises shallow marine to continental facies. The Mitole Sandstone Member was interpreted to be mainly fluvial to alluvial deposits (Hudson, 2011).

### 1.3. *Lower Cretaceous*

The Lower Cretaceous successions in the Mandawa Basin (Figs. 2 and 3) commence with the shallow marine limestones of the Nalwehe Formation (Aitken, 1961). This formation comprises a basal Limestone Member and an upper Sandstone Member, both of shallow marine affinity (Figs. 3 and 4). Outcrops of the Nalwehe Limestone Member are found in the northern part of the Mandawa Dome (Fig. 5) where they unconformably overlie Tithonian sandstones (Aitken, 1961). The Nalwehe Limestone Member is estimated to be 110 m thick (Kent et al., 1971). The Nalwehe Sandstone Member consists mainly of siliciclastic sandstones.

Whether the Jurassic depositional cycle regime continued into the Cretaceous or not still remains to be resolved. Discrepancies concerning unconformities and the earliest Cretaceous dates call for further investigation. According to the stratigraphical scheme of Hudson (2011), deposition of the Mitole Formation stretches into the Berriasian without any major depositional breaks (Fig. 3). Others argue that unconformities existed between the Tithonian and Neocomian in the central Mandawa area (Arkell, 1956; Aitken, 1961; Kent et al., 1971; Bussert et al., 2009). Based on palaeontological evidence, Arkell (1956) suggested that a widespread disconformity separates the Tithonian from the earliest Cretaceous formations, which he claimed was Hauterivian. Aitken (1961) supported this view and argued that the angular unconformities below the marine Lower Cretaceous are sufficiently widespread to confirm a hiatus. At Tendaguru Hill the Jurassic succession is separated from Lower Cretaceous (Valanginian – Hauterivian) by an erosional surface, overlain by conglomerates carrying reworked mudstones and quartz pebbles, representing a significant break in sedimentation and erosion of underlying deposits (Bussert et al., 2009).

During the Late Jurassic to Early Cretaceous, halokinetic uplift

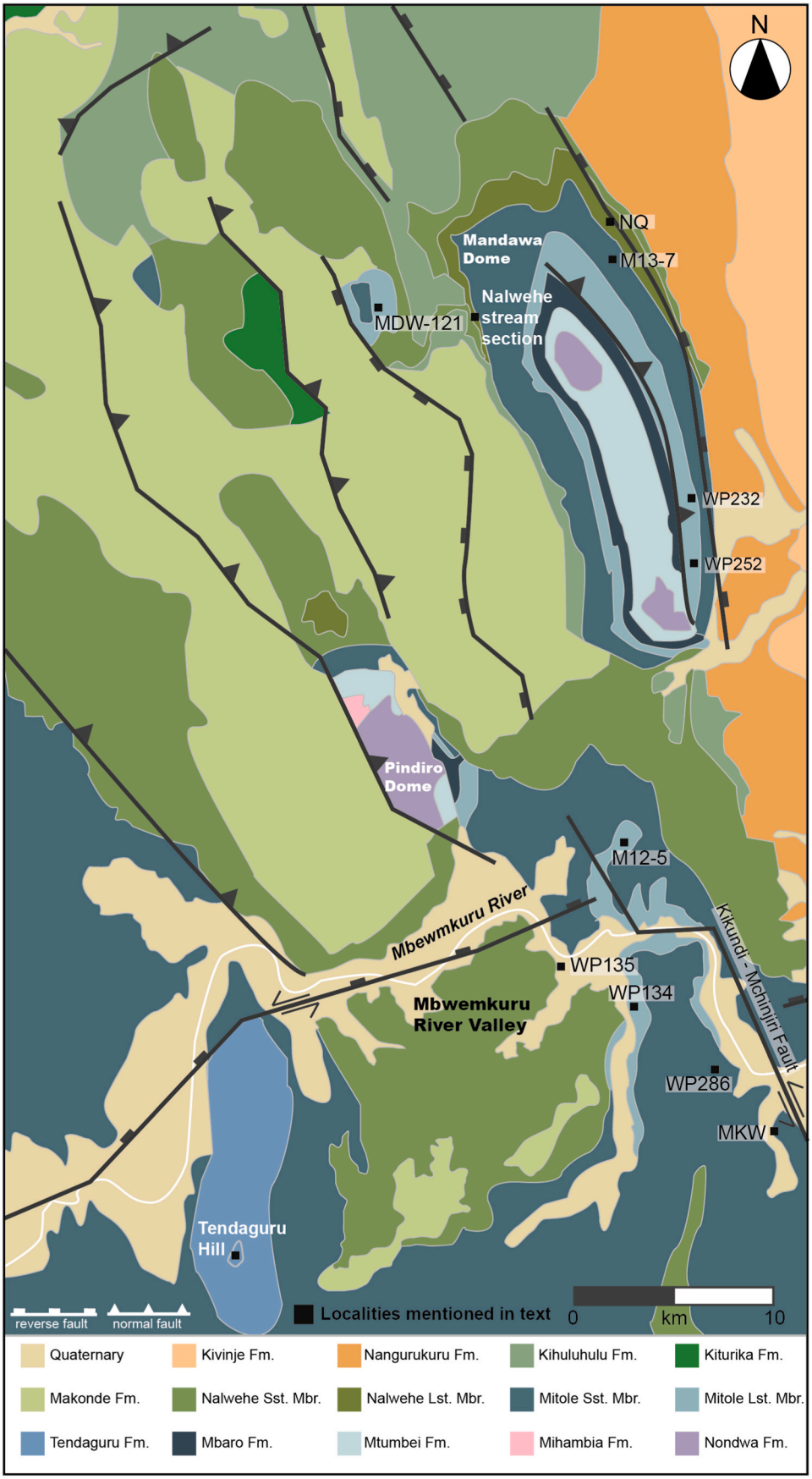


**Fig. 5.** Enlarged view of the central area of the Mandawa Basin (from Fig. 2). Modified from Hudson (2011), additional information from Aitken's geological map of central Mandawa Basin (Aitken, 1961).

occurred prior to deposition of transgressive Albian marine sediments, (Aitken, 1961; Didas, 2016). In the Kizimbani-1 well, drilled on a basement high 43 km north of the Mandawa Dome (Figs. 2), 750 m of evaporites have been emplaced between Bathonian and late Aptian strata (Balduzzi et al., 1992). Seismic interpretation shows that faulting related to the last phase of salt movement occurred from the Late Jurassic into Aptian times (Didas, 2016). The NNW trending Kikundi-Mchinjiri fault in the Mbwemkuru area (Fig. 5) appears to have been active during this period, when a sag developed west of the shear zone where Early Cretaceous deposition took place. Accommodation zones were created where the older NNW-SSE faults were intersected by E-W transfer faults associated with strike-slip displacements (Aitken, 1961). Fault gouges in supracrustal rocks in the Mbwemkuru area testify to major Cretaceous movement along lineaments here (Didas, 2016).

Both the Tendaguru and Nalwehe formations are unconformably overlain by the Aptian – Albian Kiturika, Kihuluhulu and Makonde formations (Fig. 3); a major unconformity separates them (Aberhan et al., 2002; Hudson, 2011). The Makonde Formation was first described by Bornhardt in 1900 (Quennel et al., 1956), who proposed that the formation passes laterally into the limestones of the Kiturika Formation. Aitken (1961) claimed that the sedimentological information for that correlation was rather poor. Exposures of the Makonde Formation are found throughout the coastal plateau of southern Tanzania. Similar deposits are found in Mozambique in the Ruvuma Basin (Fig. 1), where it is known as the Macomia Formation (Hancox et al., 2002; Smelror et al., 2008). The Makonde Formation (Figs. 2 and 3) has been interpreted as fluvio-deltatic deposits (Hudson, 2011; Gundersveen, 2014). The possible time-equivalent Kiturika Formation is exposed in the central parts of the basin (Figs. 2, 3 and 5) and includes gastropod and coral limestones that locally intercalate with the Makonde Formation (Quennel et al., 1956; Hudson, 2011). The Kihuluhulu Formation (Figs. 2, 3 and 5) is mainly composed of fine-grained sediments (marls and siltstones) with subordinate sandstone beds. An outer-shelf environment has been proposed for the Kihuluhulu Formation, and the intercalated sandstones are interpreted as turbiditic in origin (Hudson, 2011). The Kihuluhulu Formation is overlain by deeper marine Upper Cretaceous clays (Kent et al., 1971) of the Kilwa Group (Nicholas et al., 2006).

#### 1.3.1. Northern mandawa area

The Kipatimu Formation is the only Upper Jurassic formation present north of the Matandu lineament (Figs. 2 and 3), an area which is relatively underexplored compared to the area south of the Matandu River. The northern extension of the Kipatimu Formation is uncertain but outcrops are found in the Wingayongo area of the Rufiji Trough (Fig. 1) (Mpanju and Philp, 1994). The Kipatimu Formation has also been encountered in wells drilled in Songo Songo Island and Mafia Island to the east of the study area (Fig. 1). Well data from Mafia Island (Fig. 1) and Songo Songo (Fig. 2) showed that the Kipatimu Formation spans the Jurassic – Cretaceous boundary with a major part of the drilled successions being Early Cretaceous (Mkuu, 2018).

A Late Jurassic (?Oxfordian – Tithonian) age has been suggested for the Kipatimu Formation in the northern area of the Mandawa Basin (Stockely, 1943; Msaky, 2007; Hudson, 2011). However, a recent study by Smelror et al. (2018) suggests that sedimentation of the Kipatimu Formation continued into the Early Cretaceous.

The Kipatimu Formation in the northern area of the Mandawa Basin was estimated to be 600 m thick, and underlain by 150 m of the Middle Jurassic carbonates of the Mtumbei Formation (Figs. 2 and 3) and 230 m of basal sandstones and conglomerates (Kent et al., 1971). The Kipatimu Formation is believed to consist of fluvial and fluvio-deltaic deposits, represented by massive sandstones, often cross-stratified, intercalated with purple and green claystones and some occasional conglomerates (Stockley, 1943; Aitken, 1961; Kent et al., 1971; Gundersveen, 2014; Hudson, 2011). It cannot be correlated with any particular unit south of the Matandu Lineament, where mainly littoral to shallow marine neritic facies are found (Aitken, 1961).

## 2. Methods

The key outcrops of this study were logged and sampled during field work in the Mandawa Basin in the 2013 and 2014 field seasons. The legend to logs is presented in Fig. 6. Geographical co-ordinates of the studied sections can be found in the Supplementary material. Relatively short field seasons dictated that the sedimentological/stratigraphical investigations were aimed at sections that 1) were easily accessible with vehicles, 2) were already mapped and studied, and 3) were not too severely weathered. Tropical weathering, which today extends at least 20 m down from the present-day surface (Nicholas et al., 2006), poses a major problem in most exposed sections in the Mandawa Basin; good and continuous exposures are often difficult to find. Loosely cemented sandstones and claystones were most affected by weathering. Weathering and deep penetrating roots often obscure or disrupt sedimentary structures and loose sediments and/or vegetation can conceal parts of the exposed sections. In some cases, bedding planes, sedimentary structures and directional structures were difficult to assess.

The rock samples were analysed at the Department of Geosciences, University in Oslo (UiO). Thin sections of blue epoxy stained rock samples were studied using an optical microscope. Point counting (400 counts per thin section) was performed on key samples. The Hitachi SU5000 FE-SEM (Schottky FEG) scanning electron microscope (SEM) at UiO with a Dual Bruker XFlash30 Energy Dispersive X-ray spectrometry (EDS) system was applied in the SEM analysis. The instrument is equipped with detectors for secondary-electron images (SEI), back-scattered electron images (BSE), and cathodoluminiscence (CL). EDS was performed on carbon-coated thin sections under high vacuum with 15 kV current, whereas samples intended for surface morphology study were mounted on copper stubs and Au-coated.

Whole rock mineralogical composition was determined by X-ray diffraction (XRD) using a Bruker D8 Advance instrument at UiO. Mineral phases were quantified by applying the PROFEX software which implements Rietveld refinement (Doebelin and Kleeberg, 2015).

## 3. Results and interpretation of the depositional environments from the central area

### 3.1. Mitole Formation

#### 3.1.1. Mitole Limestone Member

The Mitole Limestone Member crops out in the central parts of the Mandawa Basin (Figs. 2, 3 and 5). It was sampled and logged on the eastern flank of the Mandawa Dome at locality WP232 (Figs. 2 and 5). Other sampling localities include: M12-5, WP134 and MDW-121 (Fig. 5). These localities have previously been described as ooid-bearing limestones (e.g. in Aitken, 1961; Kent et al., 1971; Hudson, 2011; Van den Brink, 2015), but thin section studies revealed that these limestones contain oncoids and not ooids.

Ooids are small (commonly less than 2 mm) spherical or egg-shaped carbonate coated grains, exhibiting a nucleus surrounded by an external cortex. They often exhibit regularly and concentrically laminated fabrics. Ooids can form in both marine and lacustrine settings and are associated with moderate to high energy environmental settings such as shoals (Richter, 1983; Flügel, 2004). Oncoids, in contrast, are biogenically formed (by algae or bacteria) coated grains, and commonly are larger than ooids (mm-to cm-sized), and can form in both quiet and high-energy environments. Oncoids often consist of a laminated micritic cortex developed around a nucleus, but usually display more irregular laminae than ooids (Preyt, 1983; Flügel, 2004). Oncoids have been described from marine, lacustrine and fluvial environments (Preyt, 1983).

The oncoid grains present in the studied outcrops have comparable size fraction to ooids (1–2 mm), which makes differentiation in the field

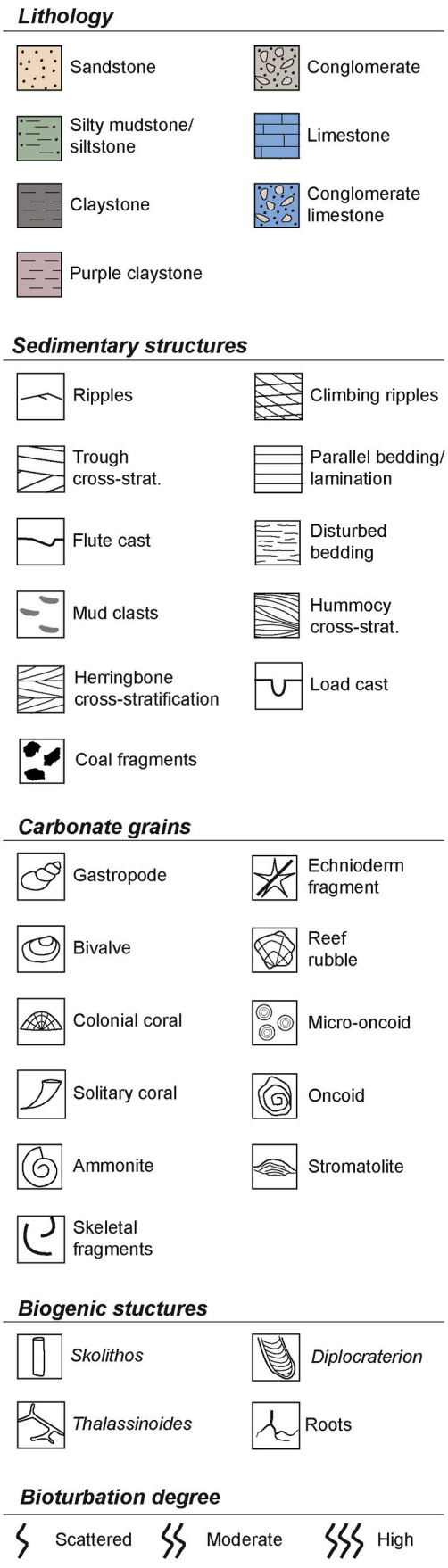


**Fig. 6.** Legend to sedimentary logs.

difficult.

### 3.2. Classification and description of limestones carrying oncoids

The limestones at localities WP232, M12-5, WP134 and MDW-121 (Fig. 5) lack depositional mud and are composed of oncoids, fragmented skeletal material, cortoids (carbonate grains with thin, non-laminated micrite envelopes) and minor amounts of quartz and feldspar in the silt to very fine sand fraction (Fig. 7). Because the limestones at M12-5, WP134 and MDW-121 contain more than 50% oncoids, they classify as oncolite (Peryt, 1981; Flügel, 2004). At the WP-232 locality, Fig. 5, the oncoids are less dominant (42–65%) and are poorly sorted due to variations in grain packing. The limestones at WP232 can be classified as oncoid-bearing grainstone (Dunham, 1962).

The exposed thickness of the oncolite at locality WP134 (Fig. 5) is 123 cm. The limestone is coarse, well sorted and cemented and contains approximately 80% oncoids. Bioclasts locally outnumber oncoids in some parts of the grainstone. No sedimentary structures, apart from a few *Skolithos* burrows, were observed. The oncolites at locality M12-5 are exposed as patches of the bedding plane cropping out on the forest floor. The observed formation thickness is only a few centimetres. No sedimentary structures were observed. The limestone is massive, well cemented with high oncoid content (70–80%). The MDW-121 locality was sampled by Hudson (2011) and was not visited during the 2013 and 2014 field campaign. The WP232 locality is described in detail later (see section 3.2.2).

The skeletal material deposited with the oncoids comprises fragmented skeletal debris with comparable or slightly greater grain size than the oncoids; mainly bivalves, gastropods, echinoderms and some indeterminate fragments. Also present are articulated foraminiferal tests, many of which are benthic species, with agglutinated, but the ecological affinity of most of the tests could not be ascertained due to low preservation and/or poor cross-sectional view. Rare ostracods and fragments of coral were also noted. The bioclasts deposited together with the oncoids seem to be the same kind of grains as those forming bioclastic nuclei in the oncoids (Fig. 7).

### 3.3. Description of the oncoids

Oncoids at localities WP232, M12-5, WP134 and MDW-121 have comparable size range and shapes, nuclei composition and lamination types (Fig. 7). The following oncoid descriptions apply to all the analysed samples.

The Late Jurassic oncoid grains in the Mandawa Basin are small (between 1 and 2 mm, Fig. 7) and fall into the micro-oncoid size range (Flügel, 2004). The majority have ellipsoidal to spherical shapes with smooth or slightly grooved surfaces (Fig. 7). Less common are elongated shapes, which are due to elongated nuclei grains, or amalgamation of two or more oncoids grains (Fig. 7d). The cortices are composed of more or less concentrically arranged laminae developed around a nucleus consisting of either a bioclast or clastic grain. One oncoid grain was found with a glauconitic nucleus. Abraded shell fragments are the most common type of nuclei; other common bioclast nuclei are foraminifera and echinoderm fragments, in addition to unidentified macro and micro-fossils (Fig. 7a and b).

Individual oncoid grains commonly display multiple lamination fabrics comprising: *i*) *Girvanella* bearing laminae, *ii*) concentric micrite laminae with constant thicknesses, *iii*) organism-bearing laminations, *iv*) discontinuous laminations with variable thicknesses (Fig. 7). Calcified micro-structures of tubular cyanobacteria (*Girvanella*) are recognisable under the microscope in some oncoids, but evident on most grains with SEM (Fig. 7e and f). *Girvanella* occur in dense concentrations within the laminae, hence identification of individual tubes is difficult under the microscope (Fig. 7g and h). A characteristic feature of *Girvanella* oncoids is the alteration of *Girvanella*-bearing and barren laminae (Peryt, 1981), as observed in several of the studied oncoids from the Mitole Limestone

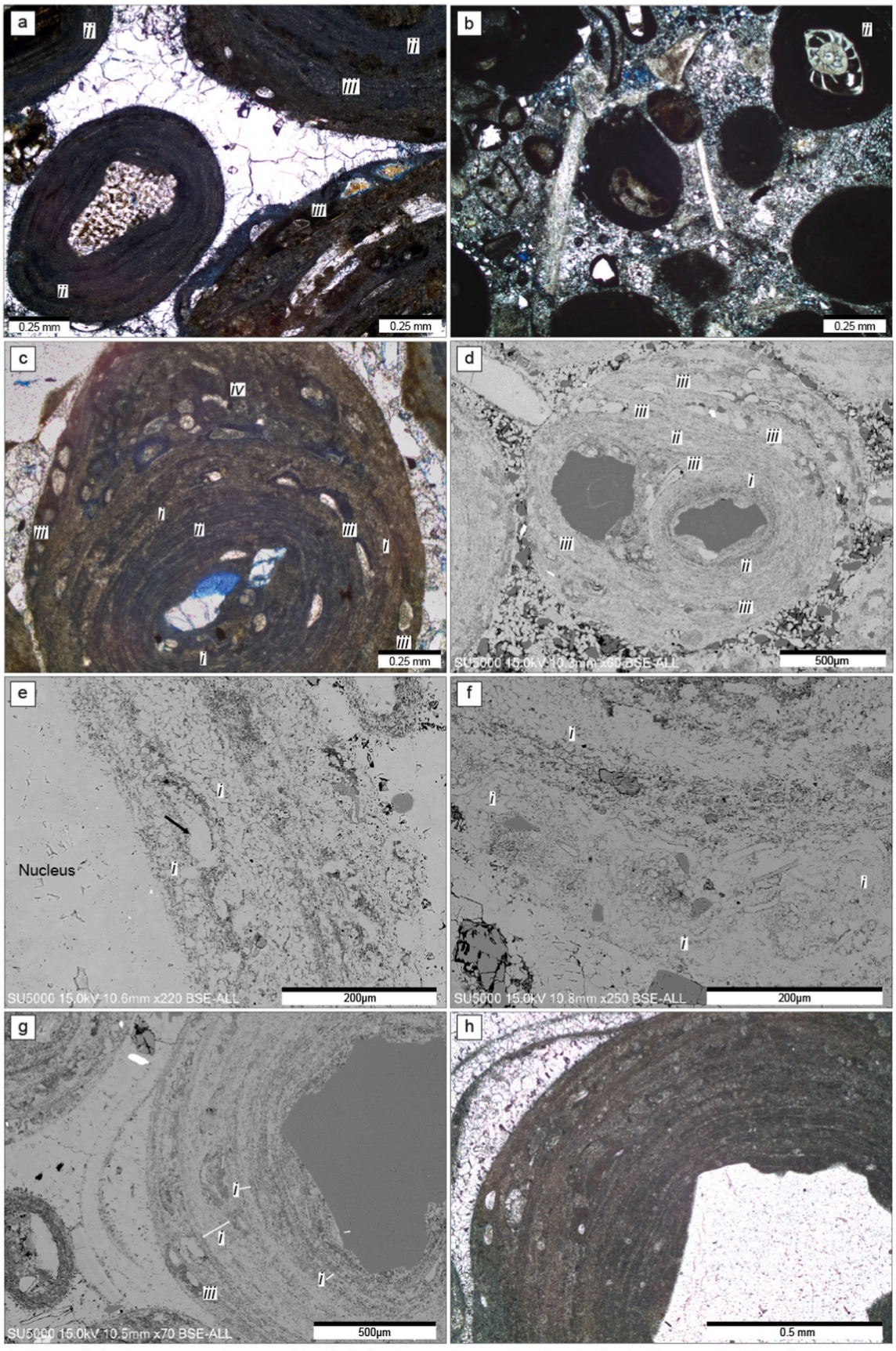


*i* - *Girvanella* lamina *ii* - concentric micrite lamina *iii* - organism-bearing lamination *iv* - discontineous lamina

*(caption on next page)*

**Fig. 7.** Thin section micrographs of oncoids from Mitole Limestone Member localities. (a) Sparry calcite cemented oncolite (WP135) viewed in plane polarized light (ppl). Small oncoid with concentric micrite laminas (*ii*) with constant thicknesses developed around an echinoderm fragment deposited together with larger, more complex oncoids with abundant organism-bearing laminations formed by *Bullapora* (*iii*). The *Bullapora* are bean-shaped, with the flat side down towards the centre of the oncoid. (b) Ppl view of oncoid and bioclastic packstone (sample WP232-4-14), blue is epoxy and represents porosity. Some oncoid grains have been broken before final deposition. (c) Elliptical oncoid grain from WP135, showing alternating lamination fabrics indicating frequent environmental changes during its formation. The inner cortex is rounded and composed of concentrically stacked *Girvanella* and micite lamina, disturbed by *Bullopora*-bearing laminations. The discontinuous laminations on the upper part the grain are more chaotic, and formed when the grain was at rest. (d) SEM image of a composite oncoid grain from sample WP232-4 composed of two intergrown grains with different lamination fabrics, note the many phases of encrustations by *Bullopora.* (e, f) Close-up views of the calcified *Girvanella* bands in an oncoid grain from sample M12-5. (g) SEM image showing fairly well preserved *Girvanella*-like tubes alternating with micrite and encrusting organism-bearing (*Bullopora*) laminations. (h) Typical appearance of *Girvanella* oncoid (sample M12-5) under the microscope in ppl where the calcified tubes are not visible (same grain as in (g)). (For interpretation of the references to colour in this figure legend, the reader is referred to the Web version of this article.)

Member. The majority of the oncoids analysed have undergone several phases of encrustation during their growth, reflected by alternating bands of encrusting organisms and barren laminations (Fig. 7). The micro-encruster inclusions were recognised as the calcareous foraminifera *Bullopora,* characterised by their occurrence as bean-shaped calcite patches, with a flat underside and a convex upper surface (Reolid and Galliard, 2007).

### 3.4. Interpretation of the environment where oncoids formed

Because the oncoids at the studied sites share common characteristics i.e. grain size, nuclei composition and lamination fabrics, formation within comparable environmental settings seems likely. The nature of cortex laminations (Fig. 7), which gives an insight into the environment in which the oncoids form, indicates frequent short-term environmental changes in energy, and perhaps even salinity variations. Oncoids formed in higher energy settings are generally sub-spherical and rounded, with thin and densely stacked concentric micrite laminations (Wright, 1983). In high-energy environments, encrustation is inhibited by constant grain rotation in agitated waters (Dahanayake, 1983). Microbial encrustation is controlled by sedimentation rates, substrate and light availability (Reolid et al., 2005; Védrine et al., 2007). Encrustation occurs during calm periods when the grain is at rest. Hence, alternating micrite and organism-bearing laminae are indicative of environments which experience alternating calm and agitated periods (Reolid et al., 2005; Védrine et al., 2007). Microbial crusts (e.g. *Girvanella*–like bands, Fig. 7e and f) grow slowly and reflect low sedimentation rates (Peryt, 1981, 1983; Leinfelder et al., 1993). *Girvanella* seems to be adapted to salinity fluctuations (Leinfelder et al., 1993). Micritic oncoids formed by constant grain rolling have been associated with agitated, protected lagoons, whereas *Girvanella*-oncoids develop in lower energy settings (Védrine et al., 2007). *Girvanella* oncoids are often reported to have been formed in marine subtidal environments during times of slow sedimentation rates, preferably in deeper rather than shallow water depths (Peryt, 1981). Bidirectional currents may form rounded and elliptical oncoids in intertidal settings where encrustation is prohibited, resulting in concentrically stacked micrite oncoids (Dahanayake, 1983). Oncoids formed in low-energy conditions are often found to be less well-laminated and have often more irregular shapes (Wright, 1983). Discontinuous laminations indicate tranquil episodes (Dahanayake, 1983).

The alternating lamination fabric common for most oncoids analysed indicates frequent and short-term environmental changes with respect to energy and clastic supply. Storms may be responsible for such periodic environmental changes. The nucleation points for many oncoids are fragmented bioclasts formed by high-energy reworking of skeletal material. Abundant echinoderm fragments are evidence for connection to the open marine environment. Storms may open and close shallow lagoons and cause short term turbulence in otherwise low-energy environments and transport skeletal material into the lagoon. The analysed oncoids are interpreted to have formed in such an environment. Several event beds (storms and possibly tsunami deposits) have been recognised from late Kimmeridgian – Tithonian strata in the Tendaguru area (Bussert and Aberhan, 2004). The small but consistent oncoid grain sizes suggest that they were prevented from growing larger. This could either be due to environmental changes which stopped further oncoid growth, or removal of oncoids from their formation environment into another area where further growth was prohibited.

### 3.5. Depositional environment of the oncolites

The oncolites at localities M12-5, WP134 and MDW-121, Fig. 5, were deposited in similar environmental settings, while the oncoid-bearing limestones at locality WP232 were deposited under different settings which will be discussed later. However, because the oncoids in the WP232 section appear similar to oncoids in the other localities, also they have been interpreted to have formed in a similar environment.

Oncoids and other carbonate grains present appear in the same size fraction, indicating pre-depositional sorting. The oncoid grains were presumably derived from mixed-energy, tidally influenced lagoons. The oncoids, together with other carbonate grains, were transported from the lagoon during storms and deposited in a high-energy environment on the inner ramp, or in shoals on the mid-ramp.

#### 3.5.1. Locality WP232

Four short sections of the Mitole Limestone Member along the eastern side of the Mandawa Dome were measured at locality WP232 (Figs. 2, 5 and 8). These sections consist of soft siltstones and resistant oncoid-bearing grainstones (Dunham, 1962). Both facies display lateral thickness variations.

The siltstones are friable, poorly sorted, partly carbonate cemented and have been more susceptible to weathering than the grainstones. Bed thicknesses in the measured sections range from 16 to 60 cm (Fig. 8). No sedimentary structures were observed in the siltstones. Oncoids and fragmented shells are randomly distributed and constitute less than 15% of the siltstone (Fig. 8).

The basal contacts of the oncoid-bearing grainstone with the siltstones are sharp and erosional, often displaying higher concentrations of oncoids, mud clasts and skeletal fragments (Fig. 8). Measured bed thickness of the oncoid-bearing grainstone was from 10 to 100 cm. Oncoids are small (less than 2 mm long) and normally constitute 30–80% of the rock. Small shell fragments were observed in all the grainstone beds, with increased abundances towards the top (Fig. 8; log 4). Due to variations in grain packing, sorting within one bed can range from poor to good, a characteristic feature of the oncoid-bearing grainstones at WP232. Some beds show normal grading, some are weakly bedded and others appear rather structureless. The uppermost grainstone beds in the analysed section (log section 4) contain more bioclasts than oncoids. *Skolithos* were found at the top of some grainstone beds (Fig. 8). Hummocky cross-stratification (HCS) was observed in log section 2 (Fig. 8). Maximum thickness of an HCS bed is 102 cm, with beds laterally thinning to north and south (Fig. 8). The base of the HCS bed is strongly erosive with abundant clay rip-up clasts and disarticulated shell fragments (Fig. 8).

### 3.6. Mineralogical compositions and petrographical descriptions

The oncoid-bearing grainstones of the Mitole Limestone Member at

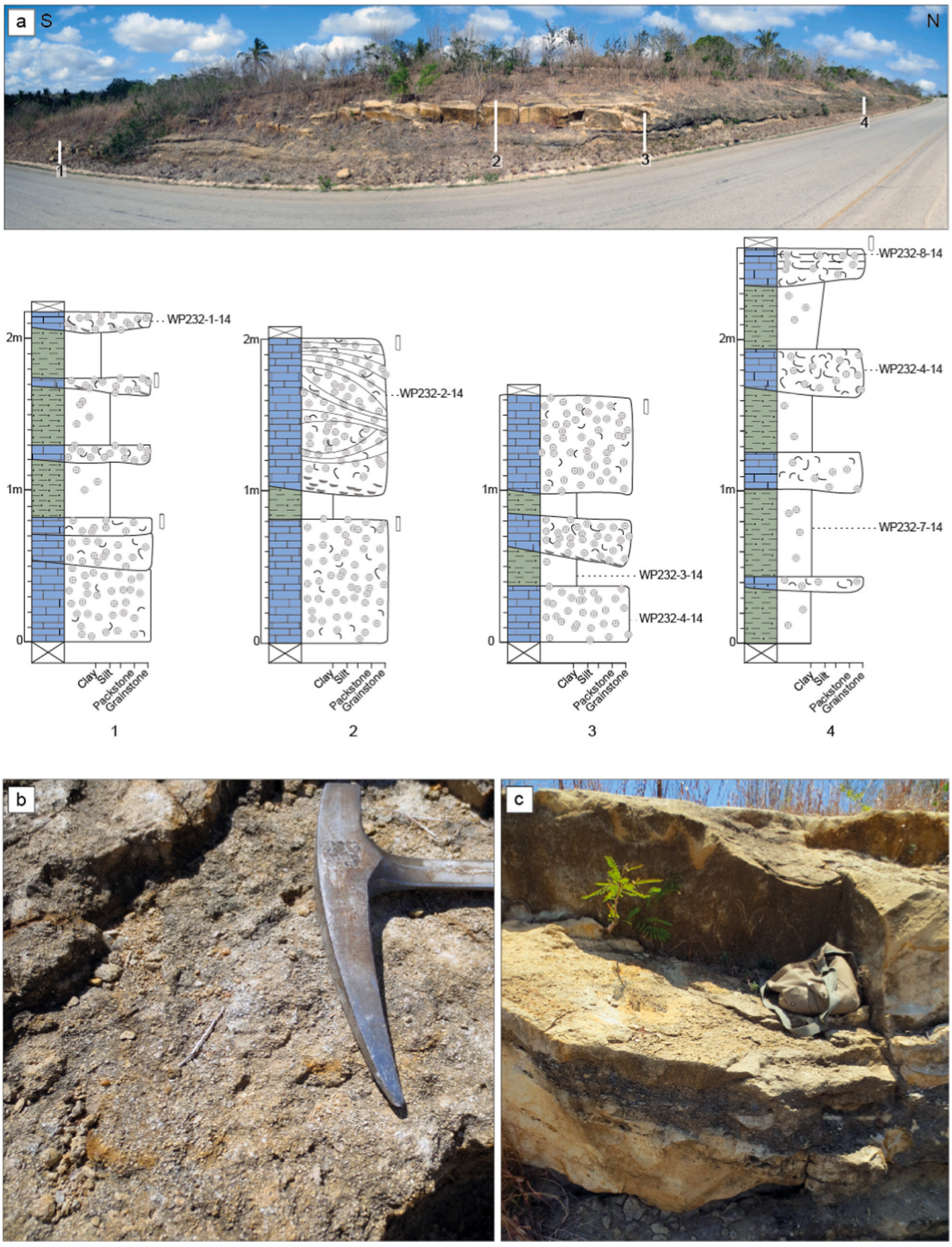


**Fig. 8.** The WP232 section of the Mitole Limestone located on the eastern side of the Mandawa Dome with interbedded oncoid-bearing grainstones and siltstones. (a) Overview of the studies section of the Mitole Limestone Member showing location of the four measured sections. (see Fig. 6 for legend to logs). (b) Typical character of the weathered surface of the oncoid-bearing limestones which previously have been misidentified as ooids. (c) Close-up view of oncoid bearing grainstone interbedded with siltstone.

locality WP232 are poor to moderately well sorted with varying amounts of oncoids, skeletal detritus and siliciclastic grains. Variations in degrees of packing observed at outcrop were also noticeable in thin sections. These grainstones are all grain supported, lacking depositional matrix, and classified as a grainstone according to Dunham (1962). Oncoids are the main framework constituent and from point counting constitute between 42 and 65% of the rock. The remaining framework is composed of skeletal detritus, cortoids, foraminifera and siliciclastic grains. The grainstones at WP232 contain fewer oncoids and display poorer sorting compared to the other oncoid localities (M12-5, WP134 and MDW-121; Fig. 5). Fossil fragments are abraded, and show only modest, if any, signs of boring or bio-erosion after deposition. The average grain size of the siliciclastic grains is in the silt to very fine sand fraction. Samples WP232-8 and WP232-6 have a high bioclastic component (20%) and a reduced amount of oncoid grains (10%) and classify as bioclastic grainstone (Dunham, 1962). Intergranular pore spaces are generally filled by sparite calcite cementation. Calcite cementation is interpreted to have been early as mechanical compaction appears to have been minimal as the majority of the grains are not in contact with each other. Thin K-feldspar overgrowths were found on both plagioclase and K-feldspar grains.

The siltstones are composed of detrital smectite and altered I/S clays (10–30%), oncoids and bioclasts (<15%), and quartz, plagioclase and K-feldspar grains in the silt fraction. The siltstones are matrix supported, poorly sorted, friable and porous. Mottling observed in the thin section analysis may be a product of bioturbation. Oncoid grain size and composition are similar to oncoids in the oncoid-bearing grainstones but are less well preserved with rougher outer surfaces, and some oncoids are broken.

The quantitative mineralogical compositions of the WP232 grainstones and siltstones are presented in Supplementary material.

### 3.7. Depositional environment

Palynological analysis of siltstone sample WP232-5-14 of the Mitole Limestone Member yielded a moderately rich and diverse assemblage of both marine and terrestrial palynomorphs (Smelror et al., 2018), where the dinoflagellate cyst assemblage shows similarities with the marine Tithonian formations at Tendaguru Hill. The siltstone facies, primarily consisting of fine-grained siliciclastics with some scattered oncoids and skeletal fragments, is interpreted to represent the local background sedimentation. The oncoid-bearing grainstones in contrast represents high-energy conditions, disrupting the more calm normal conditions.

Hummocky cross-stratification forms by oscillatory wave motion during storms, and is more likely to be preserved in water depths between fair-weather wave base and storm wave base, although HCS is not necessarily restricted to this range (e.g. Dumas and Arnott, 2006). The grainstone beds show lateral thickness variations, with beds often amalgamating along the profile, a common feature of tempestites (Flügel, 2004). Proximal calcareous tempestites are more thickly bedded than distal tempestites, coarse grained and often bioclast-rich with assemblages of mixed ecological affinity. The bases of individual storm beds are erosive (Flügel, 2004). The observed grainstones have sharp erosive bases, further advocating fairly high energy event sedimentation. All fossil fragments are abraded and show little, if any, signs of boring or bio-erosion after deposition, suggesting rapid deposition and burial in a high energy environment. Further, the ichnology of the grainstones supports the interpretation of storm bed deposition. The upper parts of tempestites are sporadically burrowed by opportunistic pioneers, commonly *Skolithos* (Pemberton and Frey, 1984; Frey and Goldring, 1992). The Mitole Limestone Member at locality WP232 is therefore interpreted to represent proximal tempestites deposited on a mid-ramp setting.

#### 3.7.1. Locality WP286

Five metres of calcite-cemented, fine-to coarse grained yellow bioclastic sandstones of the Mitole Limestone Member were measured at locality WP286 (Fig. 9a). The entire section is rich in marine fossils (such as ammonites, mussels, echinoderms and foraminifera). The eastwards facing outcrop is characterised by semi-continuous beds of calcite-cemented sandstones alternating with friable, less cemented sandstones.

The studied section contains abundant trace fossils characterised by mixed association of vertical, inclined and horizontal structures of *Cruziania* ichnofacies (*Thalassinoides*) and *Skolithos* ichnofacies (*Skolithos, Diplocraterion, Schaubcylindrichnus*). Well preserved ammonites (from 2 to 25 cm in size) were observed in the lower part of the section, and disarticulated shell fragments were noted throughout (Fig. 9a). An upwards fining, cross-stratified unit, 39 cm thick, was observed in the upper part of the section (at about level 4 m, Fig. 9a). The upper part of this unit had been bioturbated and contains trace fossils of *Skolithos* ichnofacies (mainly *Skolithos* and *Schaubcylindrichnus*). The cross-bedding displays tangential forests with 22° dip; one current measurement suggests transport towards the NE (70°). Disarticulated bioclasts and scattered coal fragments are present within this cross-stratified unit.

The mineralogical compositions and petrographic descriptions of the analysed samples can be found in the Supplementary material.

### 3.8. Depositional environment

The Mitole Limestone Member at the WP286 section is interpreted to represent deposition during moderate energy conditions operating in a fully marine environment. *Cruziania* ichnofacies is often associated with marine substrates located between minimum and maximum wave base, while *Skolithos* ichnofacies is associated with high-energy, sandy, shallow marine environments (Pemberton and MacEachern, 1995). The measured section is interpreted to represent a shallowing-upwards shoreface sequence, which during increased wave agitation deposited coarser and better sorted sediments that were more susceptible to cementation due to better permeability.

#### 3.8.1. Mitole Sandstone Member

*3.8.1.1. Locality M13-7.* The Mitole Sandstone Member at locality M13-7 on the NE of the Mandawa Dome consists mainly of yellowish-grey, moderately well sorted low-angle cross-bedded feldspathic arenites (Figs. 2 and 9b). The outcrop faces SE and the formation thickness is 2.60 m. Parts of the section are highly weathered, obscuring sedimentary structures and original grain sizes (Figs. 9c and 10d). The section commences with low-angle cross-bedded very fine sandstone, sharply overlain by coarse, low-angle cross-stratified sandstone (Fig. 9b). Low angle cross-bed dips of less than 10 deg indicate that sediment transport was towards the east. Vertical sand-filled burrows, identified as *Skolithos* and *Diplocraterion*, are common (Fig. 9b). Also noted were shell fragments and well-rounded quartz pebbles scattered throughout the section. Interbedded with the low-angle cross-stratified sandstones is a thin high-angle (30°) trough cross-stratified sandstone with tangential foresets (level 0.69–0.78 m), also displaying an easterly sediment transport. This coarse grained sandstone is poorly sorted with an erosional bounding surface to the bed below (Fig. 9b).

The mineralogical compositions and petrographic descriptions of the analysed samples can be found in the Supplementary material.

### 3.9. Depositional environment

Vertical burrows of predominately *Skolithos* indicate a moderate to high-energy depositional environment (Pemberton et al., 2012). The Mitole Sandstone Member at M13-7 is interpreted to mainly represent foreshore, high-energy depositional environments. The swash and backwash mechanism creates low-angle, seaward dipping, planar-parallel laminations in typically well sorted medium-to coarse--grained sandstones as observed at this locality (Pemberton et al., 2012).

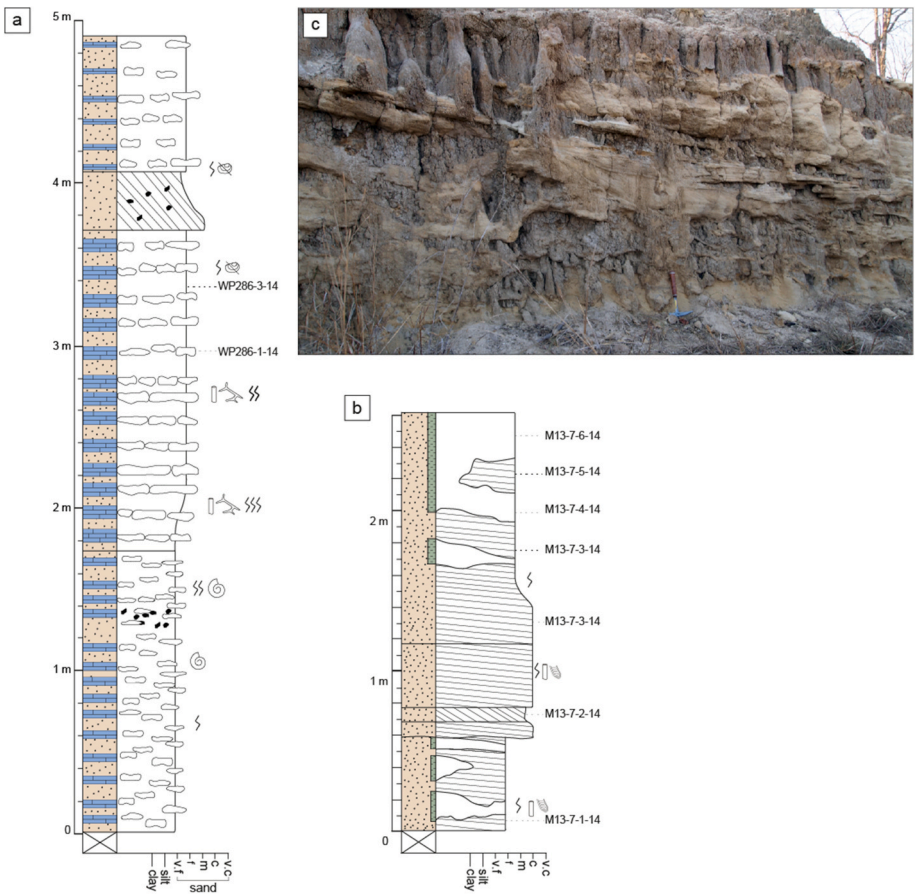


**Fig. 9.** (a) Sedimentary log of the Mitole Limestone Member at locality WP286. (b) Sedimentary log from the M13–7 section (see Fig. 6 for legend). (c) Outcrop photo of the Mitole Sandstone Member at locality M13-7, showing the poor and weathered state of the outcrop.

The erosional-based trough cross-bedded unit might represent a seaward-propagating dune deposited in the swash to surf zone transition (Clifton et al., 1971).

### 3.9.1. Locality NG

The Mitole Sandstone Member is exposed in a cliff section at locality NG, in the Matandu River Valley, where 20 m of yellowish, friable, cross- and parallel bedded subarkosic sandstones are exposed (Figs. 2 and 11). The measured section commences with cross-bedded and parallel-bedded medium grained yellow sandstones with thin (level 0–2 m) claystone interbeds (Fig. 11a). Bipolar (herringbone) cross-stratification, cross-bedding and tidal bundles with double mud drapes (Fig. 11c) and reactivation surfaces (Fig. 11b) were identified. The dominant current direction is 333° (SE).

The middle section of the Mitole Sandstone Member (level 3–7 m, Fig. 11a) is composed of cross-bedded and parallel-bedded, sandstones with some interbedded cross-stratified siltstones, but bipolar cross-sets were not observed. The grain size ranges from silt to coarse sand. Reactivation surfaces interrupt cross-strata sets with the same current direction and foreset inclination above and below the surface (Fig. 11b).

The upper part of the section (level 8.20–13.30 m, Fig. 11a) is dominated by yellow to pinkish horisontal bedded, medium grained sandstone with very thin clay beds, interrupted by a 1.6 m thick unit of cross-bedded sandstone. This cross-bedded sandstone displays planar foresets with clay rip-up clasts along the base of the bed. Palaeocurrent direction on the cross-strata is towards NE (68°).

The mineralogical compositions and petrographic descriptions of the analysed samples can be found in the Supplementary material.

### 3.10. Depositional environment

The Mitole Sandstone Member at locality NG (Fig. 2) is characterised by sedimentary structures typical of tidal sedimentation, e.g. herringbone cross-stratification, tidal bundles, mud couplets and reactivation surfaces (Visser, 1980; Davis, 2012). The bipolar cross-stratification observed in the basal part of the section (Fig. 11a) indicates deposition under fairly equal flood and ebb currents strengths (Davis, 2012). The tidal conditions change upwards in the profile deposition, where deposition under one (i.e. dominant) current direction seems to prevail. Current measurements indicate a northwards flow, likely representing a flood-oriented current. During the flood stages of the tidal cycle cross-stratified beds were deposited, where the upper part of the bed was scoured by the ebb current. The alternating sandstones and thin claystone laminations in the upper part of the section (level 8.30–13.4 m, Fig. 11) are interpreted as deposition in a shallow subtidal setting. The cross-stratified bed with mud clasts centred along the base of the bed which cut the heterolithic deposits; represent the cut and fill of a subtidal channel with dominant flow towards ENE. The horizontally oriented parallel-bedded units represent bottom set lamination.

In summary, the Mitole Sandstone Member at the NG section is interpreted to have been formed in a shallow, subtidal channel environment.

### 3.11. Nalwehe Formation

Two sections (NQ1 and NQ2) located c. 100 m apart were measured in the Nantama Quarry on the NE side of the Mandawa Dome (Figs. 2, 5, 12 and 13). At locality NQ1 both members of the formation are exposed, while at NQ2 probably only the Limestone Member is exposed (Figs. 12

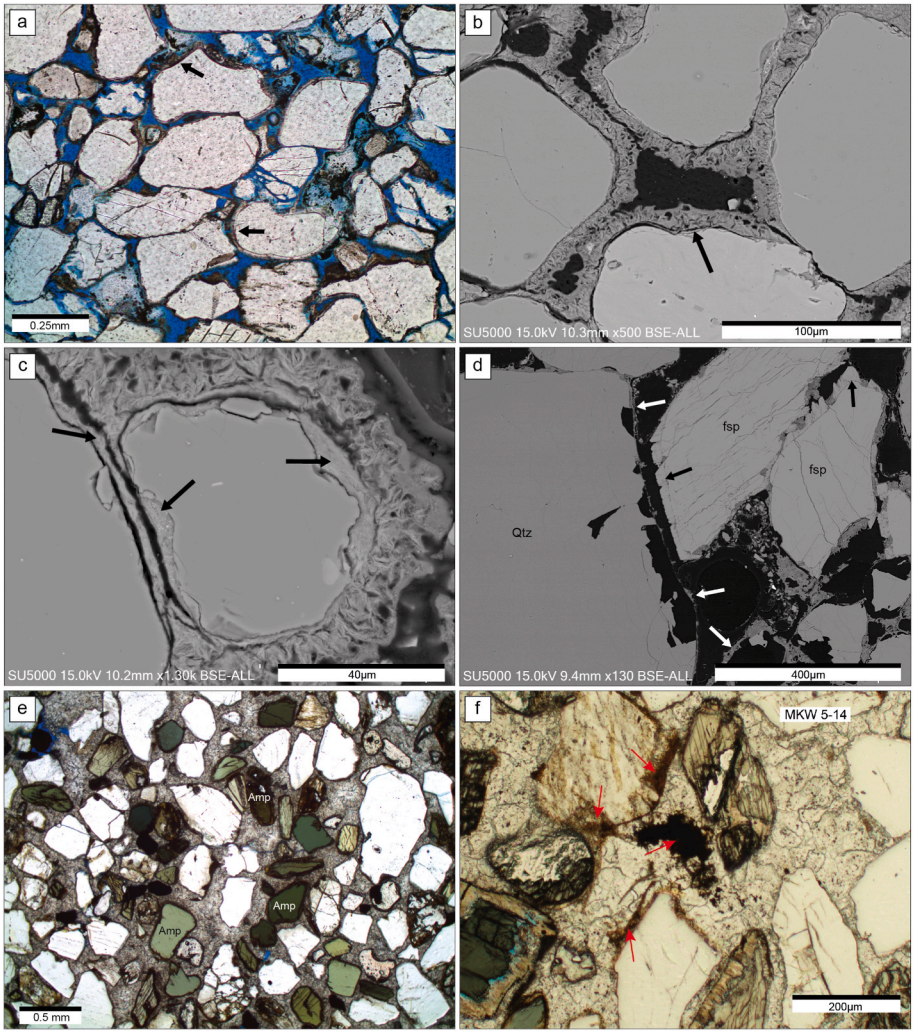


**Fig. 10.** Thin section micrographs of sandstones of the Mitole and Nalwehe formations from the central area of the Mandawa Basin. (a) Thin section photomicrograph (ppl) showing typical appearance of the Mitole Sandstone Member at locality NG (blue areas are epoxy and represent porosity). Thin clay coatings appear as brown rims around detrital grain surfaces indicated by arrows. Grain contacts are mainly long to concavo-convex. (b) SEM image, sample NG-5-13, showing authigenic interstratified chlorite-smectite coatings. The chlorite-smectite precursor was identified as inherited smectite coating, indicated with arrow. (c) Close-up view of the precursor smectite rim and authigenic chlorite-smectite coating, sample NG-5-13. (d) SEM image of the Mitole Sandstone Member, sample M13-7-3-14, showing a weathered fabric. Feldspar grains are found with partially dissolved K-feldspar overgrowths (black arrows). Dissolution of the framework grains is evident by the isolated smectite coatings (white arrows) where the nucleation grains have been lost. (e) Ppl view of Nalwehe Sandstone Member sample MKW5-15. The sandstones at locality MKW are enriched in amphibole (greenish grains) and have low porosities due to early diagenetic calcite cementation. Grain contacts are floating to tangential. (f) Bitumen was found in the sandstones at locality MKW in places where calcite and amphiboles are corroded. (For interpretation of the references to colour in this figure legend, the reader is referred to the Web version of this article.)

and 13a, b). Maximum formation thickness in the quarry is roughly 20 m, however the top 10 m show a gradual transition of saprolised sandstone into red soil (Fig. 13).

### 3.11.1. *Locality NQ1*

The NQ1 section displays shallow marine carbonates overlain by clastic shallow marine facies (Figs. 12a and 13a). The measured section commences with grey bioclastic mudstones overlain by wackestone (level 0–2 m, Fig. 12a). Further up the bioclast content increases, grading into bioclastic packstone (Fig. 12a). In the upper parts of the Limestone Member (level 4.6–6.3 m, Fig. 12a) articulated fossils and corals (solitary and colonial) are found in life position and there are numerous patches of recrystallised colonial corals. The top packstone is characterised by a highly irregular, karstic upper surface. The cavities in this surface were later filled and capped with coarse bioclastic sand (Figs. 12 and 13a), which forms a contact between the two members. The overlying Nalwehe Sandstone Member at NQ1 consists of clay-cemented, friable sandstones with some scattered, coal-like fragments, alternating with thin bioturbated, carbonate mudstones. The top of the measured section (level 8.20–9.30 m, Fig. 12a) comprises cross-stratified sandstones, which have a foreset dip of about 8°, indicating current flow direction wastowards E (355°).

## 3.12. *Mineralogical compositions and petrographical descriptions*

The Nalwehe Formation limestones are classified as bioclastic wackestones to bioclastic packstones (Dunham, 1962). In thin section, the mudstones, wackestones and packstones are seen to be dominated by micrite and various amounts of bioclastic debris, some broken but not abraded. The most common fossils are bivalves, echinoderms, gastropods, sponges, corals, foraminifera and crinoids. The carbonate grains often have thin micritic envelopes and some fossils have been bored (*Trypanites* ichnofacies). Sparite cement is found within fossils and fissures or as a pore-filling phase, and the amount of sparite increases towards the top. Sparite-cemented fissures cutting through fossils and matrix were seen in all samples, while framboidal pyrite and dolomite growth zonation were observed in SEM images of mud- and wackestones (level 0–2 m). Dolomite was detected by XRD in all limestone samples (0.3% average). Rhombohedral dolomite crystals with growth zonation was detected with SEM in sample NQ1-1-14.

The transitional sandstone (NQ1-6-14, Fig. 12a) is sparite-cemented (35%) and poorly sorted, with subangular to rounded clastic grains with tangential contacts. The friable sandstones of the Nalwehe Sandstone Member above (level 6.4 m, Fig. 12a) are poorly to moderately well sorted arkosic, calcite-free and clay-rich wackes, (17% smectite). Quartz and feldspar grains are common in the very fine sand fraction; they display subangular to subrounded morphology with tangential to long contacts. Plagioclase and K-feldspar grains have K-feldspar overgrowths in samples NQ1-6-14 and NQ1-7-14. Only a few tiny shell fragments were observed. Thin section from a calcite-cemented bed display a calcite-cemented bed (NQ1-8-14, Fig. 12a) display a matrix-supported texture of siliciclastic grains in the silt to very fine sand fraction,

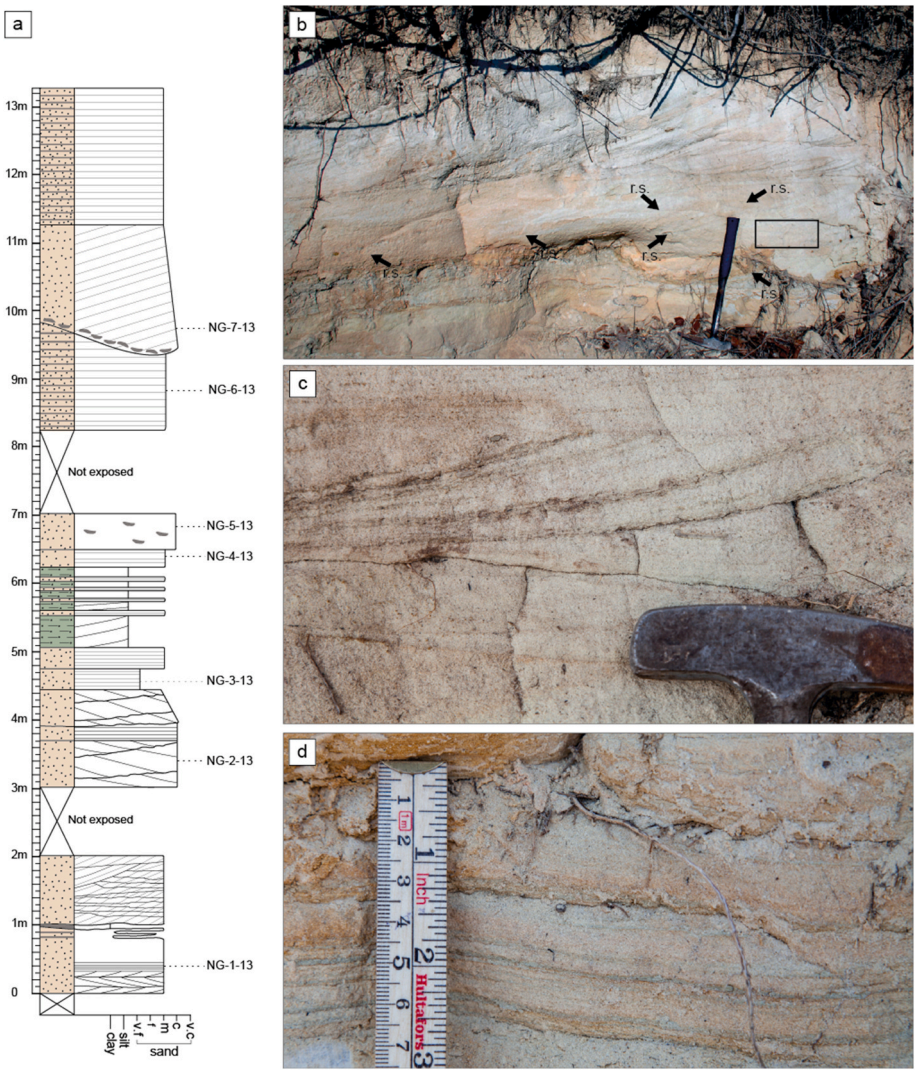


**Fig. 11.** The Mitole Sandstone Member at locality NG. (a) Sedimentary log of the studied section, see Fig. 6 for legend. (b) Cross-stratified sandstones with mud draped tidal bundles separated by reactivation surfaces (r.s.). (c) Close-up view of b) showing a mud draped tidal bundle. (d) Tidal bedding.

floating in micrite and fine grained sparite. The detrital grains are mainly quartz and feldspar, but in addition contain abundant mica and heavy minerals. The rock is mainly composed of calcite (80% volume) and classifies as mudstone. Thin section analysis revealed chaotic bioturbated fabric and burrows filled with sparite calcite.

Mineral phase quantification of the collected samples can be viewed in Supplementary material.

### 3.13. Depositional environment

The presence of micrite envelopes indicates deposition within the photic zone, and the high content of depositional micrite mud suggests a generally low energy environment. Hypoxic to anoxic water conditions are also partly indicated by the presence of framboidal pyrite in sample NQ1-1-14, Fig. 12a (Berner, 1984). The mudstone (level 0–1 m, Fig. 12a) is interpreted to have been deposited in a restricted lagoon that experienced changes in the Mg/Ca ratio of the seawater as a result of periodic influx of freshwater.

The overlying wackestone/packstone unit (level 1–4 m, Fig. 12a), with more bioclasts and sparite cement, suggests deposition in a more agitated part of the lagoon. Disarticulated fossils in the lower part of the NQ1 section (Fig. 12a) were probably transported into the lagoon during storms. The presence of small patches of *in situ* corals in the upper part of the limestones may reflect presence of patch reefs in the distal parts of the lagoon. In summary, the Nalwehe Limestone Member at the NQ1 section displays a transgressive development from a low energy, inner ramp restricted lagoon into open marine mid-ramp setting with patch reefs.

The irregular surface of the top limestone (level 6.4 m, Fig. 12a) is interpreted as a karstic surface produced by vadose dissolution during subaerial exposure (Wright, 1982). This surface might be the Barremian unconformity which is postulated to separate the limestone and sandstone members of the Nalwehe Formation (Hudson, 2011). A basinward shift in facies during the Early Barremian has also been suggested by Sansom (2016).

No fossils were observed in the Nalwehe Sandstone Member overlying the open marine lagoonal facies. A fairly low-energy depositional environment is inferred for the sandstones at level 6.4–8.20 m (Fig. 12a) from the high content of depositional mud (up to 50%). The lack of sedimentary and biogenic structures in this section make further elaborations on the depositional environment challenging. From the homogeneous sandstones and towards the top of section (8.20–9.40 m, Fig. 12a), alternating low-angle cross-stratified sandstones intercalate with carbonate mudstones. This part of the section is poorly exposed due to weathering of the sandstones and hard to access due to exposure elevation. Only one sample (NQ1-8-14) was collected from this part of

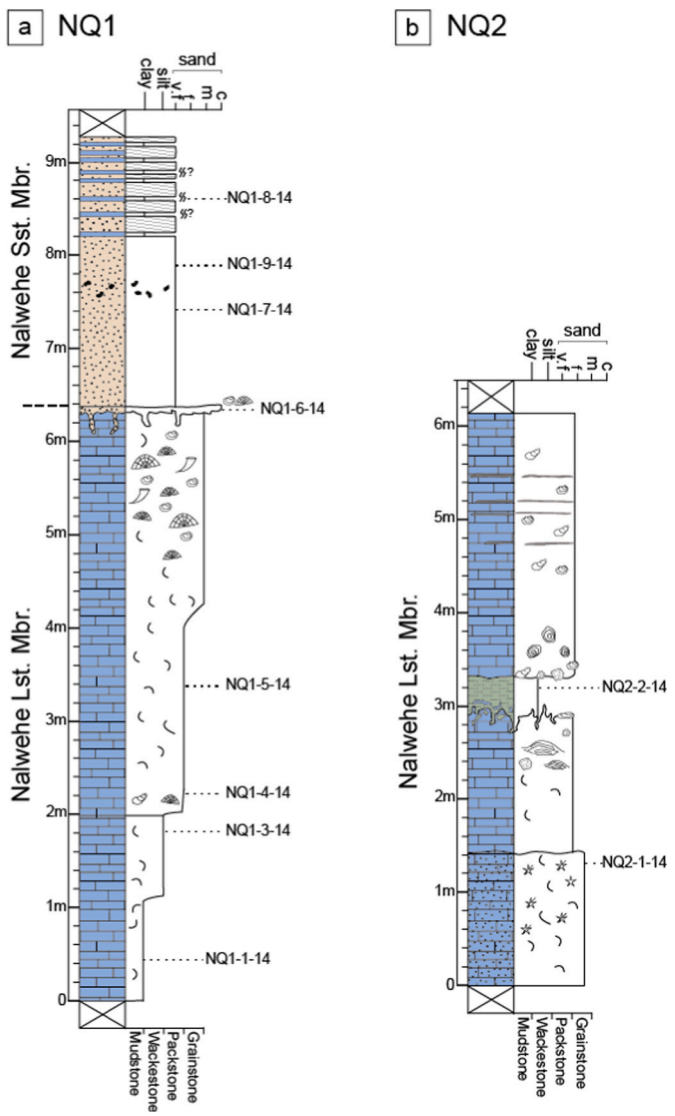


**Fig. 12.** Sedimentary logs of the Nalwehe Formation in Nantama Quarry (see Fig. 6 for legend to logs). (a) Section NQ1 with the basal limestone member, and the upper sandstone member. (b) Section NQ2 is interpreted to only represent part of the limestone member.

the section, hence the environmental interpretation is rather sketchy. The carbonate mudstone does not contain any macrofossils, but the bed is bioturbated. The dominance of micritic mud over sparite calcite suggests calm water deposition for the mudstones. The low-angle cross-beds with landward-dipping foresets might represent small washover fans into a backshore lagoon or coastal lake (Schartz, 1982).

### 3.13.1. Locality NQ2

Six metres of the Nalwehe Formation were measured at locality NQ2 in the Nantama Quarry (Figs. 12b and 13b). The internal stratigraphical relation of NQ2 relative to the NQ1 section was not resolved due to complex, local faulting.

The NQ2 section commences with 142 cm of friable, poorly sorted, medium-grained calcareous sandstone overlain by packstone (level 1.4–3 m, Fig. 12b). The packstone appears bedded, showing alternating well-cemented, discontinuous beds that are more resistant to weathering, interbedded with more friable and softer sediments (Fig. 13b). Well rounded pebble-sized grains and calcite intraclasts are present in the packstone. In the upper part of this section (2.3–3 m, Fig. 12b) a dome-shaped structure interpreted as a stromatolite was observed (Fig. 13c). The top of the packstone is characterised by an undulating irregular karstified surface onto which thick-shelled oysters in life position were cemented (Fig. 12b). Overlaying the packstone is 40–50 cm of poorly sorted, dark grey siltstone, which in turn is covered by almost 3 m of packstone (Figs. 12b and 13b). A few discontinuous clay stringers were noted in the upper part of the section (Fig. 12b). Big elliptical oncoid grains (12–13 cm long) occur along the base of the packstone (Fig. 13d).

### 3.14. Mineralogical compositions and petrographical descriptions

Thin section analysis of sample NQ2-1-14 (Fig. 12b) revealed grain-supported, moderately well sorted, sparite-cemented siliciclastic grainstones rich in echinoderm fragments and rounded mudstone clasts. Non-carbonate grains are coarse-to medium-grained, rounded to subrounded with tangential grain contacts. Carbonate cement was determined to be 34%, fossil fragments (mainly of echinoderms) make up 12.5% of the volume. Fossil fragments are abraded, without micrite envelopes or borings. The sandy siltstone (sample NQ2-2-14, Fig. 12b) displays a poorly sorted, matrix-supported fabric. Subangular to rounded quartz and feldspar grains are mainly in the silt fraction but medium to coarse sand grains are also common.

### 3.15. Depositional environment

The NQ2 limestones differ from the lagoonal and reefal limestones of the Nalwehe Limestone Member observed at the NQ1 locality. The increased components of siliciclastic material indicate closer proximity to a siliciclastic source, which could be located proximally or laterally. The lower grainstones occurring at level 0–1.4 m (Figs. 12b and 13b) are high-energy deposits, inferred from the absence of any depositional mud and the marked abundance of abraded skeletal fragments of mainly echinoderms. The grainstones are interpreted as sandy shoals on the wave-agitated inner ramp.

The depositional setting of the packstones that overlie the grainstones (level 1.4–3 m, Fig. 12b) has not been resolved. No samples were collected from this section, hence microfacies analysis was not preformed. The interpretation of this unit is therefore mainly based on the occurrence of a stromatolitic structure found in its upper part (Fig. 13c). Stromatolites are laminated sedimentary structures formed by microbial organisms (Krumbein, 1983; Stolz, 2000). The occurrence of dome-shaped stromatolites in the upper part of the bed perhaps indicates a microbial origin for the well-cemented sections that may resemble microbial mats (Fig. 13c). Microbial mats can develop in the intertidal and subtidal zones given the right conditions in which the benthic community is dominated by microbes during times of low sedimentation rates (Browne et al., 2000; Stolz, 2000).

The top of the stromatolitic packstone is highly irregular, suggesting subaerial exposure, or intense boring of a lithified substrate (hardground). This irregular surface might be a product of karstification as observed at NQ1, possibly formed during the same event. The oysters found cemented in life position colonised the lithified packstone surface prior to deposition of the poorly sorted, dark grey siltstone (Fig. 12b), suggesting a break in sedimentation. The palynomorph assemblage of sample NQ2-2-14 is dominated by mainly terrestrial flora and *Tasmanites* sp. (Smelror et al., 2018). This suggests deposition close to the shoreline, possibly in marine waters with somewhat restricted circulation. As no fossils were observed in the thin section of the siltstone, a highly stressed environment is suggested for its deposition. The packstone above the siltstone carries large oncoid grains, gastropods and a few articulated bivales, which suggest a still somewhat stressed depositional environment, with variable salinity (Flügel, 2004), e.g. an intertidal setting. Based on the current data, the Nalwehe Formation at the NQ2 section is interpreted to represent a shallowing-upwards sequence from a subtidal to an intertidal depositional setting.

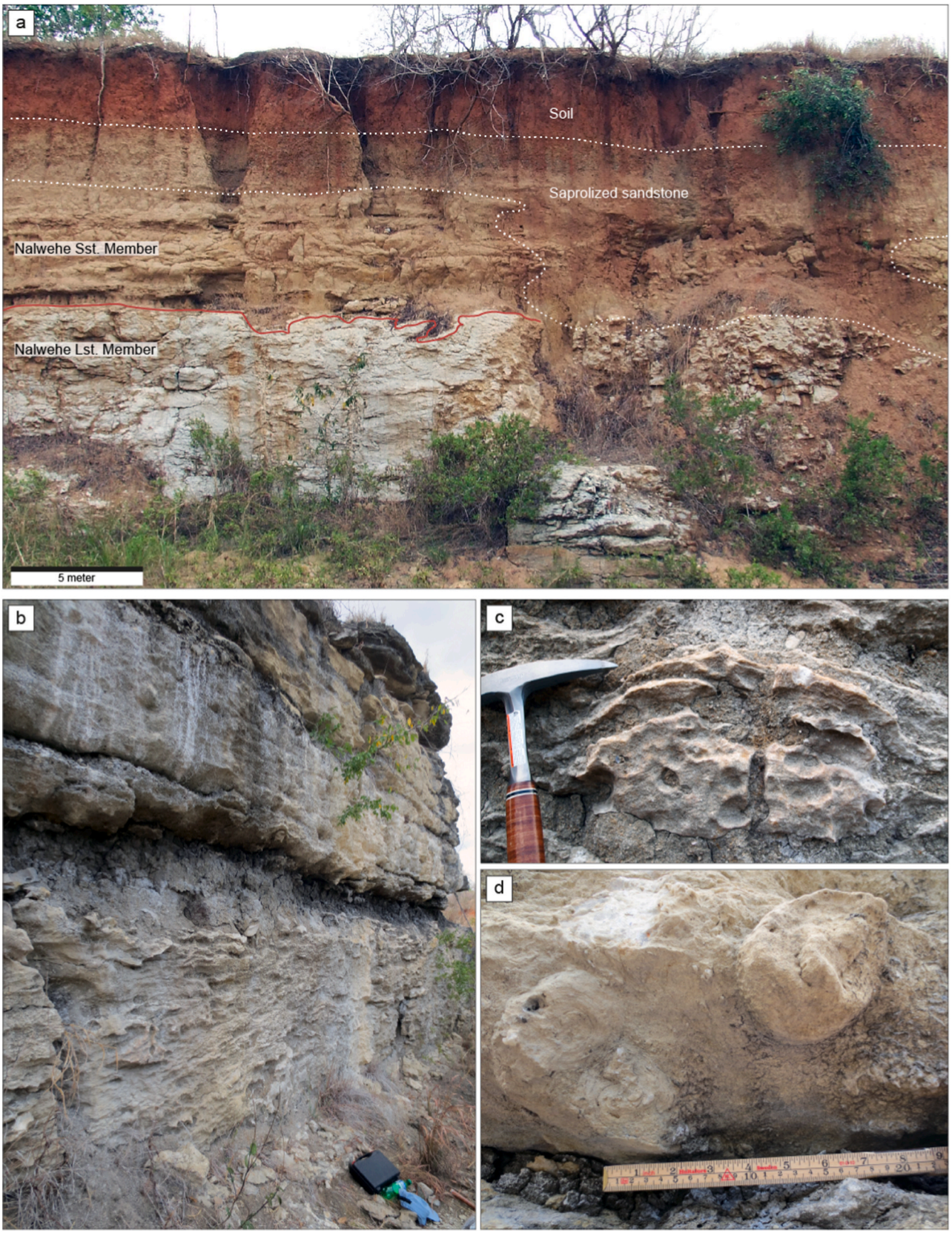


**Fig. 13.** Outcrop photographs from Nantama Quarry, where the Nalwehe Formation is exposed. (a) Photograph displaying the studied NQ1 section. The light grey limestones are not as affected by weathering as the upper sandstones, which are saprolised at the top. Note the karstified surface between the Nalwehe Limestone Member and the Nalwehe Sandstone Member. (b) View of the NQ2 section. (c) Interbedded stromatolite and packestone. (d) Two large oncoid grains in packstone.

### 3.15.1. Locality MKW

The Nalwehe Sandstone Member is exposed in a cliff section carved out by one of the tributaries of the Mbwemkuru River at locality MKW (Figs. 2, 5 and 14). The formation thickness here is approximately 11 m and consists of grey, carbonate-cemented, fine-to coarse grained, trough cross-bedded feldspatic sandstones which are conglomeratic in parts (Fig. 14). The section is comprised of several upwards-fining, trough cross-beds with conglomeratic erosive bases, locally interbedded with parallel laminated units (Fig. 14).

The mineralogical compositions and petrographic descriptions of the analysed samples can be found in the Supplementary material.

## 3.16. Depositional environment

The few fossil fragments of echinoderm and bivalve observed in the sandstone indicate deposition in a marine-influenced environment. Angular grain shapes and immature sediment composition suggest a short transportation distance. A heavy mineral study by Fossum et al. (2018) suggested the neighbouring Masasi Spur to the west (Figs. 1 and 2) was the main sediment source for the MKW sandstones. The high intergranular volume (IGV), loose grain packing and the well preservation of amphiboles (Fig. 10e) reflect rapid and shallow burial. The minor variations in chemical compositions of both amphiboles and garnets present suggest minimal mixing with sand grains derived from other sources (Fossum et al., 2018). This implies deposition occurred in an area protected from longshore currents and coastal reworking. Other amphibole-rich sandstones carrying the same provenance signatures are restricted to an area within the Mbwemkuru River valley and in the southern part of the Mandawa Dome (localities WP135 and WP252, Fig. 5).

The strong dominance of fluvially-derived sediments and their localised areas may represent delta or bay-head delta deposition, or perhaps sedimentation within a river-dominated estuary. In river-dominated estuaries, the inlets are maintained by a high fluvial discharge and fluvial sediments often extend out to the coastal barrier. Due to strong wave activities, the ebb tidal delta often can be poorly developed, and flood tidal deltas are often small or absent (Cooper, 2002).

## 4. Results and interpretation of the depositional environments from the northern area

### 4.1. Kipatimu Formation

### 4.1.1. Locality MN

At locality MN about 30 m of weathered and friable red sandstones of the Kipatimu Formation is exposed (Figs. 2 and 15). The outcrop preservation is only moderate due to the friable nature of the sandstone beds. The upper part of the section comprises red, saprolised sandstone grading upwards into soil (Fig. 15a). Furthermore, vertical digger marks produced by excavator machines have obscured sedimentary structures (Fig. 15a). Bed architecture and the lateral relationships were not resolved due to the poor state of the weathered outcrop and abundant loose sediment cover.

The 20.5 m thick section commences with a 2 m thick tripartite sequence comprising 0.7 m of thick grey claystone, erosively overlain by

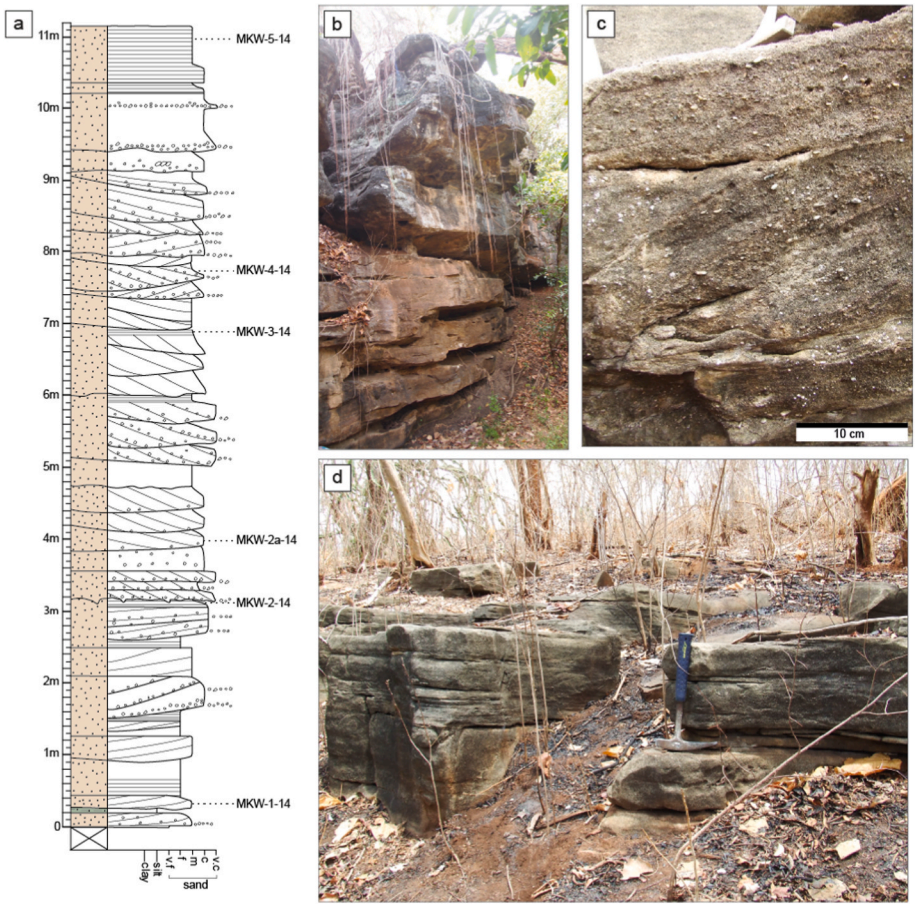


**Fig. 14.** (a) Sedimentary log of the Nalwehe Sandstone Member at locality MKW, showing mainly coarse grained, trough cross-bedded lihofacies (see Fig. 6 for legend). (b) Typical appearance of the outcrops, which due to the high content of calcite cements are well preserved. (c) Trough-cross-bedded sandstones, partly conglomeratic. (d) The upper metre of the section, showing planar bedding structures (sample MKW5-14).

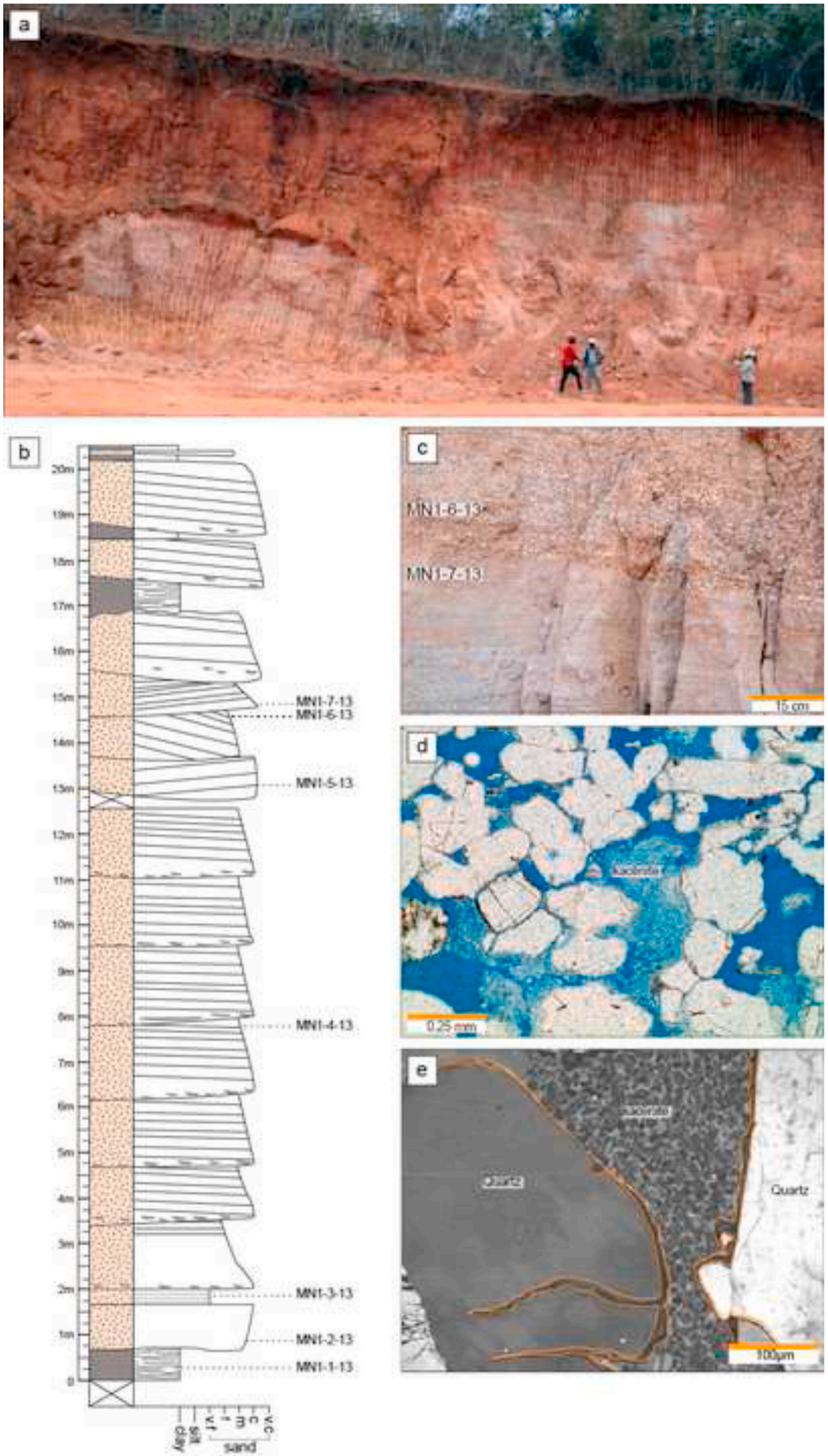


**Fig. 15.** (a) Overview of parts of the exposed Kipatimu Formation at locality MN displaying the typical red and weathered appearance characteristic of the studied section. (b) Composite sedimentary log of the Kipatimu Formation, see main text for description, and Fig. 6 for legend. (c) Close-up view of the boundary between trough cross-bedded sandstones at level 14.25–15 m (d) Typical appearance of the blue epoxy stained thin sections showing highly porous sandstones with well-crystallized kaolinite booklets clearly visible. (e) Thin quartz overgrowths (marked in orange) on quartz surfaces and within fractures. Note the thick pore-filling kaolinite between the two quartz grains. (For interpretation of the references to colour in this figure legend, the reader is referred to the Web version of this article.)

1 m of upwards-coarsening medium to coarse sandstone, followed in turn by 0.3 m of well sorted, very fine grained, light grey laminated sandstone (Fig. 15b). The laminated sandstone is succeeded by a generally poorly exposed, 10.5 m thick unit consisting of seven sets of very low-angle to near horizontal, planar tabular cross-beds (level 2–12.5 m, Fig. 15b). Each set, roughly 1.5 m thick, is an upwards-fining, coarse-to medium-grained sandstone with sharp, planar contacts with underlying beds. Pebble-sized grey clay clasts are concentrated along the base of each set (Fig. 15b).

The 10.5 m thick co-set of cross-bedded sandstones is overlain by 3.75 m of trough cross-bedded sandstones, in turn succeeded by large-scale high-angle, cross-bedded coarse sandstone with some light grey claystone intercalations (level 16.75–20.5 m, Fig. 15b). The contact between the trough cross-bedded sandstones and the underlying low-angle stratified co-set was partly obscured (Fig. 15b), but appears to have been a gently scoop-shaped erosional surface. The top 3.5 m of the measured section is composed of planar tabular cross-beds with foresets dips of about 30°, with some claystones intercalated. The top of the section was not accessible but, studied from afar, appears to be more clay-rich than the beds below, with thin claystones deposited on top of cross-beds (Fig. 15b). Palaeocurrent measurements on the cross-beds throughout the section indicate a dominant and fairly consistent flow towards ENE.

The mineralogical compositions and petrographic descriptions of the analysed samples can be found in the Supplementary material.

### 4.2. Depositional environment

The planar and trough cross-bedded lithofacies, which together account for the 2–16.75 m interval, are interpreted as bar deposits of a sandy, braided river (Collinson, 1970; Smith, 1972; Miall, 1977; Cant and Walker, 1978). The 10.5 m thick co-set makes up half of the studied section (Fig. 15b). The near-horizontal bedding is interpreted to represent deposition in the upper flow regime. Longitudinal bars, which are elongated parallel to the flow direction, are characterised by massive or crude horizontal bedding, formed by migrating planar sheets under high flow conditions (Rust, 1972). The low-angle cross-sets are interpreted to represent migration of longitudinal planar sheets in shallow water during high intensity flow events. Alternatively, the 10.5 m thick co-set might represent ephemeral river deposits with each set representing deposition during a single flash flood (Miall, 1977; Stear, 1985).

The trough cross-bedded sandstones (level 13–16.70 m, Fig. 15b) are interpreted as channel filling by 3D dune migration (Miall, 1977; Cant and Walker, 1978). The overlying high-angle cross-beds are interpreted as migrating linguoid or transverse bars where the planar-tabular cross-bed formed by avalanche-slope progradation gives rise to the high depositional foreset angles (Miall, 1977). The uppermost claystone beds (level 16.75–20.5 m, Fig. 15b) possibly represent channel abandonment or flood-plain sedimentation (Miall, 1977).

In summary, the fluvial deposits of the Kipatimu Formation observed at locality MN are interpreted as representing a large sandy, braided (ephemeral?), fluvial channel characterised by migration of planar sand sheets and bars, and associated channel cuts and fills. The resulting deposits consist of moderately well sorted, permeable sandstones, susceptible to meteoric flushing, where kaolinite precipitated as unstable phases dissolved (e.g. feldspar, heavy minerals and micas). The diagenetic kaolinite with well-crystallized booklet stacks occludes primary pore spaces or is found as mineral replacement phase in dissolved grains.

#### 4.2.1. Locality WP92

Approximately 25 m of sandstones, claystones and conglomerates are exposed in a drainage gully along the road (Figs. 2, 16 and 17). The lower part of this Kipatimu Formation section (0–6.3 m, Fig. 16) commences with pinkish-white friable siltstone overlain by purple and greenish-grey claystones. The sandstones above are yellowish-red, barren of both fossils and bioturbation (1.75–4.5 m, Fig. 16). These sandstones are fine to coarse grained, planar laminated or trough cross-bedded. Some beds are carbonate-cemented, some are not. Palaeocurrent measurements on trough cross-bedding were 60°–240°. The planar laminated and trough cross-bedded sandstones are overlain by an 18 cm thick, coarse-grained, mudclast-rich sandstone with some rare *Skolithos*-like burrows (sample bed WP92-6-14, Fig. 16). The mudclast-rich sandstone is succeeded by 20 cm of fine-grained, poorly sorted, bioturbated and fossiliferous sandstone (WP92-7-14). Articulated bivalves were observed on the bed surface. Also noted were abundant rounded mud clasts. The fossiliferous sandstone is succeeded by 130 cm of light, greenish-grey clays in turn overlain by a 20 cm thick, carbonate-cemented trough cross-bedded sandstone with irregular contact to the clays below. The sandstone is overlain by a 25 cm thick alternate bedded dark grey and brownish-grey claystone (Figs. 16 and 17a).

The middle part of the section (level 6.3–9.8 m, Fig. 17a) consists of conglomerates and sandstones. The 1-m thick basal conglomerate is grain-supported, with a coarse to medium-grained sandy matrix. The contact with the claystone below is wavy and sharp (Figs. 16 and 17a). The conglomerate is polymictic and contains a variety of intrabasinally derived clasts. Most abundant are yellow sandstone clasts, including boulders up to 53 cm long. Other common clast types include: siliciclastic and carbonate mudstones, and well-rounded clasts of quartz, chert and basement lithologies. Fossils or bioturbation were not observed.

The basal conglomerate is overlain by an upwards fining, medium to fine-grained, friable pinkish sandstone with scattered mudclasts and claystone stringers. The conglomerate was already lithified when the overlying sand was deposited, as no sand seems to have sieved down. The contact between the conglomerate and sandstone is very sharp and irregular (Figs. 16 and 17b). The friable pinkish sandstone is in turn overlain by a second conglomerate bed (30 cm thick) with structural characteristics similar to those of the first conglomerate, but with smaller clasts. The conglomerate is overlain by sandstone with similar characteristics to the bed below but with a bioturbated upper part. The sandstone is succeeded by 50 cm of bioturbated greenish-grey claystone and 75 cm of fine-grained yellowish sandstone with discontinuous claystone lenses, possibly disturbed by bioturbation which is visible in the upper part of the bed.

The upper two-thirds of the measured section (level 9.8–24.7 m, Fig. 16) is dominated by partly laminated silty claystones, intercalated with cm thin beds of very fine sandstone and a few thicker and coarser sandstone beds. The topmost unit is a carbonate conglomerate bed. This part of the section is less well exposed than the lower and middle sections. Consequently, the geometry of the thin sandstones beds here was not resolved; most beds display lateral thickness variations, some are clearly discontinuous and appear to be sandstone lenses (Fig. 17c). The interbedded silty claystones display alternating dark grey and brown laminations. Laminations in parts of the sections are disturbed, possibly by bioturbation. However, the poor preservation of the claystone does not allow either the type or degree of bioturbation to be resolved. Two thicker sandstones beds were found in the lower part of the upper section: the lower bed (level 12.25–12.50 m, Fig. 16) has disturbed parallel laminations and displays minor bioturbation, whereas the upper bed (level 12.6–13.25 m, Figs. 16 and 17d) is homogenous at the base, parallel-laminated in the middle part and displays climbing ripples at the top, suggesting a SE current direction (320°).

The alternating very fine sandstone and silty claystone unit ends at approximately level 22.6 m and is overlain by dark grey pure claystones (Fig. 16). The contact between the two lithologically different units was not exposed. The topmost thin sandstone bed at level 23.20 m (Fig. 17e) is fine-grained and ripple laminated. This sandstone is in turn overlain by 135 cm of seemingly homogenous dark grey claystone.

The Kipatimu Formation at locality WP92 is overlain by a carbonate conglomerate bed of approximately 60 cm thickness. The conglomerate is calcite cemented and bioturbated, and as opposed to the conglomerate beds below it contains abundant articulated bivalves and gastropods.

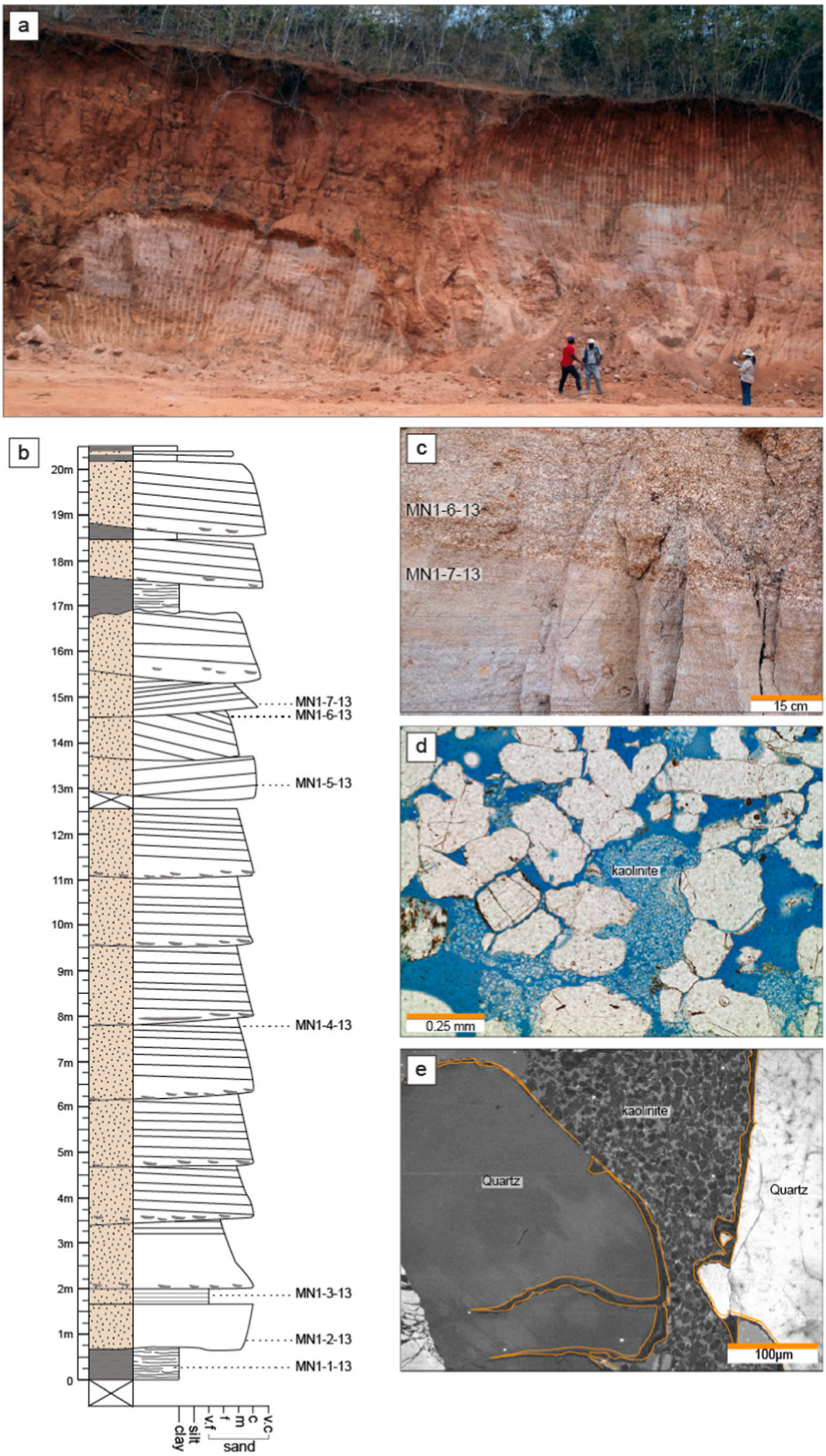


**Fig. 16.** Composite sedimentary log of the Kipatimu Formation at locality WP92, composed of clays and sandstones in the lower part of the section (level 0–6.3 m), conglomerates and sandstones in the middle part of the section (level 6.3–9.8 m), and laminated silty claystones, intercalated with thin sandstone beds at the top (level 9.8–24.7 m). The section is capped by a conglomeratic limestone.

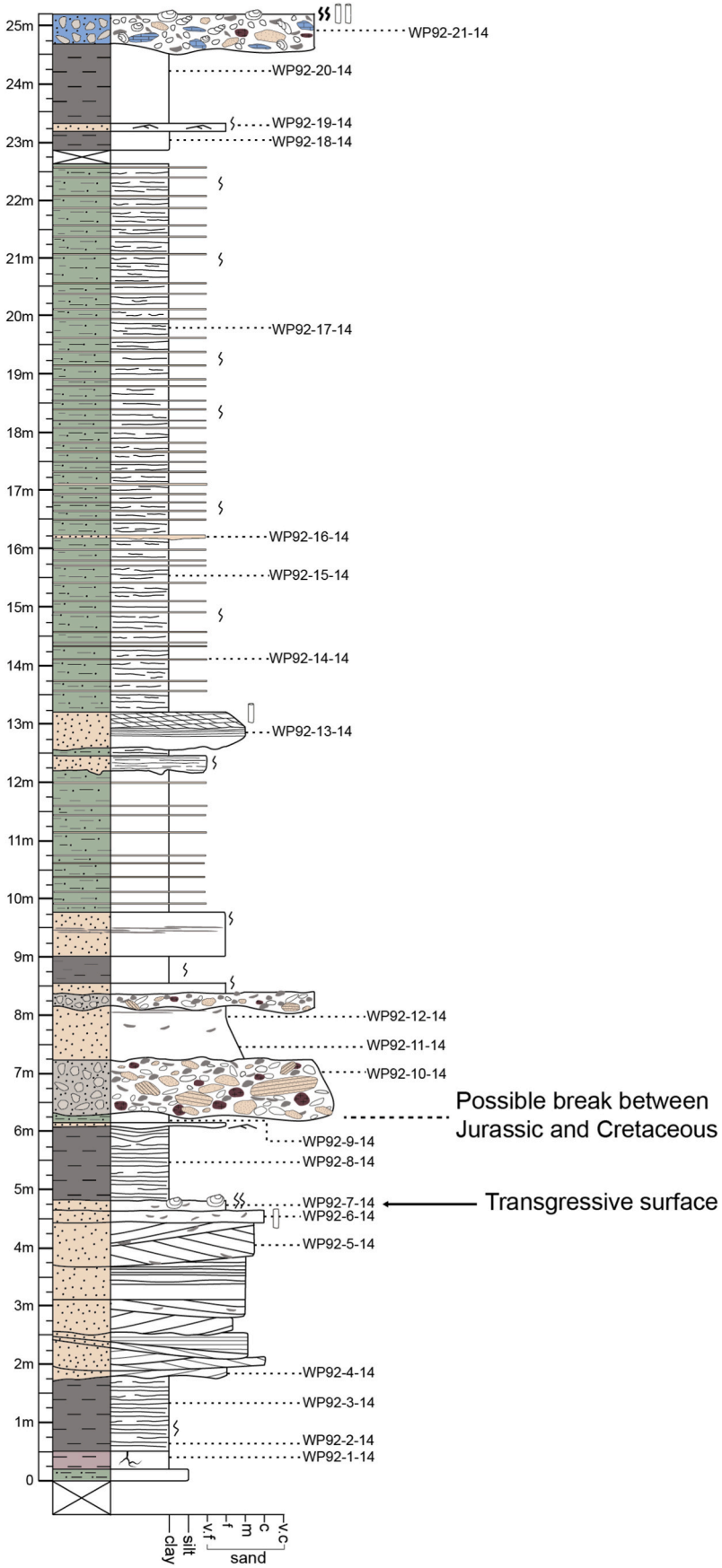


**Fig. 17.** Field photographs from the WP92 section. (a) Photo of the 5.5 m–6.75 m interval of the measured section showing the contact between the claystones of the lower section and the conglomerate of the middle section (Fig. 6). (b) Photo displaying the sharp and irregular boundary between a conglomerate bed and the overlying sandstone bed at 7.25 m (arrows). (c) Typical appearance of the alternating claystones and sandstones in the 13.5 m–22.5 m interval of the WP92 section. The thin interbedded sandstone beds appear to be discontinuous, resembling lenticular bedding. (d) View of sample bed WP92-13-14 showing parallel and climbing ripple lamination. (e) Shallow current ripples preserved on the bedding plane of sample bed WP92-19-14 at 23.25 m.

The conglomerate clasts are mainly of sedimentary origin, both siliciclastic and carbonate.

A short walk up a nearby hill revealed an overlying massive reefal and fossiliferous limestone c. 10 m thick. The age of these limestones are uncertain as no dating has been performed. However, based on its stratigraphic position between the Lower Cretaceous at WP92 and Upper Cretaceous clays of the Kilwa group these limestones might belong the Aptian Kiturika Formation, and represent a major transgressive surface in the northern area of the Mandawa Basin.

The mineralogical compositions and petrographic descriptions of the analysed samples can be found in the Supplementary material.

### 4.3. Depositional environment

The purple claystone with well-preserved root structures (level 0.5 m, Fig. 16) indicates terrestrial deposition, possibly on a floodplain, away from marine influence. The overlying well-bedded green claystones were not studied in detail, but palynomorph analysis of sample WP92-3-14 revealed only terrestrial flora and freshwater algae (Smelror et al., 2018). Based on the palynomophs present, a terrestrial depositional setting is also suggested for sample WP92-3-14. The laminated claystones were most likely deposited in a lake on the coastal plain, fed by small rivers.

The origin of the overlying trough cross-stratification and parallel laminated sandstones is challenging to decipher due to limited lateral exposures of the section. Based on the mineralogical and petrographical differences between samples WP92-4-14 and WP92-5-14 a change in depositional conditions is inferred to have occurred prior to deposition of the trough cross-stratification and parallel laminated sandstones; the content of depositional mud seems to increase upwards. There is also an upwards increase in mud clasts in the sand unit (2–4 m, Fig. 16). The trough cross-bedded unit may represent small fluvial channels on a coastal plain environment, or tidally influenced migration of 3D dunes.

The first evidence of marine sedimentation in the section is seen in sample WP92-7-14 (Fig. 16). The rock is characterised by its high content of reworked lithoclasts of mostly mudstone and contains faecal pellets and ooids, which can be can be found in both marine and lacustrine settings (Freytet and Verrencchia, 2002) but echinoderm fragments in the sample advocate a marine origin for the carbonate grains. The high content of reworked lithoclasts and the first appearance of marine organisms reflect a transgressive development. The transgressive surface appears to underlie the bed with sample WP92-7-14. The overlying claystone level 4.6–6.1 m (sample bed WP92-8-14, Figs. 17 and 18a) is dominated by diverse terrestrial sporomorph assemblage with only one single observation of marine algae, *Tasmanites* sp., indicating restricted marine depositional conditions (Smelror et al., 2018). The claystones might therefore represent lagoonal sediments. Sample WP92-9-14 (Figs. 17 and 18a) sampled just below the first conglomerate was barren of marine palynomorphs; it contained only one single terrestrial sporomorph (Smelror et al., 2018), and might represent closing of the restricted lagoon and the formation of a coastal lake environment (regressive development).

The two conglomerate beds (at levels 6.3–7.25 m, and 8.15–8.4 m, Fig. 16) are lithologically similar. This suggests that emplacement of the two conglomerate beds may have been initiated by the same event, perhaps transgressive reworking or tectonically induced mass

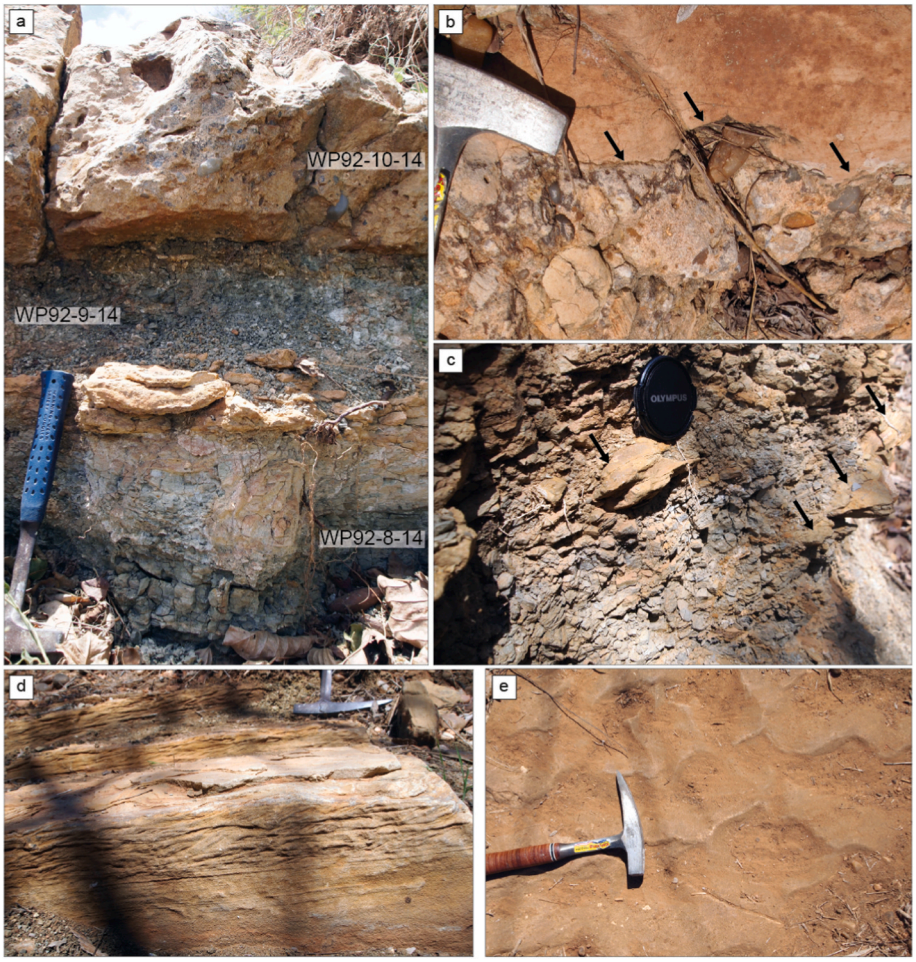


**Fig. 18.** Stratigraphic summary diagram showing the relative ages, relationship and depositional setting of localities discussed in the text.

movements. The presence of rounded glauconite grains, indicates a supply of marine material, suggesting deposition during transgression.

Chert occurs both as large clasts and as sand-sized grains dispersed in the matrix, and is found in smaller amounts in all the sandstone samples above the conglomerates. The abundant chert clasts may be derived from Karoo rocks, which are known to contain silicified wood and chert, e.g. Kandawale sub-basin to the west (locality MP, Fig. 2) and/or the Rufiji Basin to the north (Stockley, 1935, 1945; Hudson, 2011; Nerbråten, 2014). Sandstone clasts are abundant in the conglomerates and appear mostly as fine-grained reddish-yellow sandstones. The sandstone clasts were probably sourced from within the basin, possibly from Karoo strata, or from older parts of the Kipatimu Formation. The conglomerate bed reflects high energy conditions and extensive reworking of older strata.

The alternating silty claystone and thin, very fine grained, sandstone lenses were deposited in an environment with frequent, repetitive changes in energy. The poorly exposed upper section (level 9.8–23.7 m, Fig. 16) is dominated by partly laminated silty claystones intercalated with thin very fine-grained sandstone beds. The silty claystones are poorly exposed in the section and appeared devoid of sedimentary structures; if originally present, these have since been destroyed by bioturbation and/or weathering. The thin sandstone beds appear as discontinuous lenses showing lateral thickness variations, resembling lenticular bedding (Reineck and Wunderlich, 1968). The thin bedded, very fine-grained sandstone beds seemingly occur at regular intervals, perhaps caused by tidally controlled cyclic deposition of sand and silty clays. In such tidal settings, finer sediments are deposited during the slack stages in the tidal cycle, whereas sand transport and deposition occurs in between. The result is lenticular/wavy or flaser bedding depending upon the mud to sand ratio (Reineck and Wunderlich, 1968; Wang, 2012). The discontinuous sand lenses resemble lenticular bedding, hence, the heterolithic upper section is interpreted as tidal deposits, possibly of an intertidal flat. The thicker sandstone bed (e.g. sample WP92-13-14, Figs. 17 and 18d), which grades upwards from massive to planar laminated to climbing-ripple laminated facies, is interpreted to be deposited by landward (flood) oriented currents.

Palynological analyses performed on some of the interbedded claystones (samples WP92-14-14 and WP92-17-14, Fig. 16) suggest deposition in the proximity of the terrestrial environment (Smelror et al., 2018). Highest marine diversity was found in sample WP92-14-14 where *Tasmanites and Leiospaeridia* sp. occur together with some fern spores. The marine species indicate a restricted marine environment with reduced bottom water circulation and partly anoxic conditions (Smelror et al., 2018). The sporomorph assemblage in sample WP92-17-14 consisted mainly of fern spores and conifer gymnosperm spores plus undetermined marine forms (Smelror et al., 2018). The terrestrial sporomorphs present were derived from vegetation typically adapted to lowland and coastal settings (e.g. vegetated plains, freshwater swamps and marshes), which may or may not have been subjected to short episodes of marine flooding (Abbink et al., 2004).

The uppermost claystones (level 2.85–24.75 m, Fig. 16) appear less silty. Claystone sample WP92-20-14 contains only terrestrial flora (*Araucariacites autralis)* and freshwater algae (*Botryococcus*). The palynomorph assemblage testifies to a change in depositional setting form marginal marine to terrestrial. A lacustrine depositional environment is therefore implied. The carbonate conglomerate does not belong to the Kipatimu Formation. The conglomerate resembles beach rock deposits and likely represents a major transgression. The overlying reefal limestones were deposited after the transgression.

## 5. Correlation of the Kipatimu Formation

Most of what is known of the Kipatimu Formation (Fig. 3) is based on well data, mainly from Songo Songo, where it spans the Jurassic – Cretaceous boundary (Mpanda, 1997; Mkuu, 2018). Unfortunately, no detailed lithofacies descriptions or sedimentary logs have been published from the Songo Songo wells, nor any sequence stratigraphic or depositional framework models. The Kipatimu section in the Songo Songo-1 well has been interpreted as mainly representing deltaic depositional conditions; the Middle to Upper Jurassic successions represent deltaic alluvial plains, and the Lower Cretaceous represents deltaic deposits (Mpanda, 1997). It is reasonable to speculate that the braided river deposits of the MN section developed in connection with the Middle Jurassic – Upper Jurassic deltaic, alluvial plain deposits encountered in the Songo Songo boreholes (Mpanda, 1997; Mkuu, 2018).

Onshore, the sandy and non-fossiliferous fluvial section of the Kipatimu Formation has proved challenging to date. The depositional age is largely inferred from its stratigraphic position between the Bajocian – Bathonian Mtumbei Formation and Aptian – Albian marine marls (Stockely, 1943; Hudson, 2011). Kent et al. (1971) suggested that deltaic sedimentation of the Kipatimu Formation occurred immediately after the Bathonian. This is in agreement with Sansom (2016) who recognised stacked, progradational fluvio-deltaic and shallow marine deposits within the offshore Callovian – Oxfordian sequence. The fluvial sedimentation of the Kipatimu Formation is therefore more likely to have occurred prior to or during the time of deposition of the Lower Dinosaur Member of the Jurassic Tendaguru Formation within the Callovian – Oxfordian.

The Kipatimu Formation at locality WP92 spans the Jurassic – Cretaceous boundary (Smelror et al., 2018), deposited prior to the major Albian transgression. Several disconformities might be present in the WP92 section, but due to poor age control recognition of these unconformable contacts is difficult.

The lower parts of the WP92 section bears lithological similarities to the Dinosaur members of the Tendaguru Formation as described by Bussert et al. (2009). We propose that deposition of the lower part of the section (level 0–1.75 m, Fig. 16) was contemporaneous with the Lower Dinosaur Member. The trough cross- and parallel-bedded sandstones (level 1.75–4.6 m, Fig. 16) are tentatively correlated with the Nerinella Member of the Tendaguru Formation based on lithofacies similar to those described by Bussert et al. (2009). The thin sandstone where sample WP92-7-14 was collected (Fig. 16) is the first clear evidence of deposition in a marine environment and can be interpreted as representing a transgressive surface within the lower part of the WP92 section. The occurrence of micritcised grains and a few broken ooids in sample WP92-7-14 indicates deposition during times of carbonate production, tentatively the late Kimmeridgian to early Tithonian transgression. Ooids were not observed during micro-facies analysis of the Mitole Limestone Member, indicating that ooid shoals were located elsewhere outside the central Mandawa area. The palynomorph assemblage in the overlying marine mudstones (sample WP92-8-14, Figs. 17 and 18) has been roughly correlated to the mid-Oxfordian – Tithonian (Smelror et al., 2018). The overlying terrestrial mudstones are regressive, possibly deposited contemporaneously with the regressive Mitole Sandstone Member and the Upper Dinosaur Member (Fig. 4).

The timing and cause of the conglomerate sedimentation are uncertain. The conglomerates possibly indicate transgressive reworking and/or tectonically induced deposition. Thus, the occurrence of rounded glauconite grains dispersed in the matrix suggests transgressive reworking. This may be related to a transgression that occurred during the Early Cretaceous (Kent et al., 1971). A transgressive conglomerate bed has been recognised in the Lower Cretaceous Rutitrigonia bornhardti-schwarzi Memberat Tendaguru Hill that was interpreted to represent the basal part of an Early Cretaceous transgressive systems tract (Bussert et al., 2009).

6. Late Jurassic to Early Cretaceous evolution of the Mandawa Basin.

### 5.1. Late kimmeridgian – tithonian

During late Kimmeridgian, the low energy siliciclastic lagoons and tidal flats of the Mbaro Formation and the Middle Dinosaur Member

were transgressed and overlain by shallow marine calcareous sandstones and carbonates (Fig. 3). The late Kimmeridgian – Tithonian transgressive sequence is marked by the first incoming beds of limestone, previously termed the smeei Oolite (Aitkin, 1961), coinciding with the base of the Mitole Formation (Hudson, 2011). Based on the new data presented herein, we propose the type section of the "*smeei* Oolite" (WP232) and other known "*smeei* Oolite" localities (WP135 and M12) (Fig. 5), to be reclassified as micro-oncolites.

In this study, the analysed micro-oncoids are interpreted to have been formed in lagoons which, at least periodically, were connected to the open marine environment. During storms, the oncoids, together with other carbonate grains, were transported from the lagoons and deposited elsewhere (both land- and basinward) as thin beds of well-sorted oncoid-bearing grainstones. The studied sections at WP232 are interpreted as tempestites deposited in water depths below fair-weather wave base but above the storm wave base. The WP232 sections demonstrate that frequent storms were occurring on the ramp margin during late Kimmeridgian – Tithonian, well in agreement with the interpretation of the Indotrigonia Africana Member of the Tendaguru area (Bussert and Aberhan, 2004). The silty facies interbedded with the grainstones represents normal background sedimentation. The siliciclastic material was probably introduced by larger rivers, e.g. to the northeast, and distributed along the coast by longshore currents, which only locally affected coastal carbonate production in the Mandawa Basin.

Oncoids are often found at the base of transgressive successions and on maximum flooding surfaces (Védrine et al., 2007), which seems to be the case in the Mandawa Basin as well. Low sedimentation rates, especially during maximum flooding, often favour the development of microbial crusts (Bádenas and Aurell, 2010), and *Girvanella* oncoids have tentatively been regarded as an indicator of slow sedimentation rates (Peryt, 1981). The presented data supports the idea that the Upper Kimmeridgian – Tithonian period was characterised by reduced rates of sedimentation accompanied by high degrees of bio-erosion and encrustation (Aberhan et al., 2002). Furthermore, the depositional environments were dominantly high-energy, causing frequent sediment reworking. Several event beds (tempestites and possibly tsunamites) have been recognised in the Indotrigonia Africana Member (Aberhan et al., 2002; Bussert and Aberhan, 2004; Bussert et al., 2009). This is in agreement with the presented interpretation of the Mitole Limestone Member.

The Mitole Limestone Member at locality WP286 contains abundant marine fossils such as ammonites and echinoderms, and were deposited under open marine conditions. Micro-oncoids were not observed in the limestones at WP286, suggesting deposition after microbial production ended, possibly in a falling stage systems tract.

#### 5.1.1. Tithonian

During the Tithonian sea-level began to fall, and carbonate production ended. Strata deposited during this time include the Upper Dinosaur Member of the Tendaguru Formation and the Mitole Sandstone Member (Figs. 3 and 4). The Mitole Sandstone Member can be recognised as a siliciclastic dominated succession. Examples from the present study include foreshore (locality M13-7) and tidal channel (locality NG) deposits (Fig. 18). The Mitole Sandstone Member is locally characterised by smectite clay cement and grain coatings. In the Njinjo area just south of the Matandu lineament (Fig. 2) the NG section is interpreted to represent tidal deposits. In the future additional outcrops in this area should be investigated, but based on current information subtidal channel environments or a tidally influenced estuarine depositional setting seem likely. This in contrast to a previous interpretation where a fluvial to alluvial depositional setting for the Mitole Sandstone Member has been proposed (Hudson, 2011).

### 5.2. Early Cretaceous

Based on interpretations of the Nalewhe Limestone Member, semi-protected lagoons existed in the back ramp and/or inner ramp areas in the Hatuerivian. As with the transgressive Mitole Limestone Member, microbial sedimentation occurred during the Early Cretaceous transgression too, forming oncoids and stromatolites at locality NQ2. Micro-oncoids, on the other hand, have not been observed in Cretaceous strata, possibly indicating that the Early Cretaceous experienced more stable depositional conditions with less event sedimentation allowing microbial crusts to grow larger structures. The Nalwehe Limestone Member at the NQ1 section represents a transgressive development from a protected lagoon with reduced water circulation to open lagoonal sediments, finally overlain by reefal limestones that may represent highstand conditions. Evidence of a subaerial unconformity (dissolution and karstification) was observed on the top of the limestone, predating deposition of the Nalwehe Sandstone Member. Data from offshore wells have suggested that significant depositional breaks have occurred within the Hauterivian (Sansom, 2016), which perhaps resulted in the unconformity observed at the NQ1 section between the two members of the Nalwehe Formation, and in the NQ2 section.

The Early Cretaceous is mainly recognised as a regressive period in coastal Tanzania (Kent et al., 1971; Mpanda, 1997). However, transgression occurred locally in the Mandawa Basin in the Early Cretaceous, establishing shallow marine environments suitable for corals, echinoderms, molluscs, stromatolites and oncolites to flourish (Aitken, 1961; Kent et al., 1971; Mpanda, 1997; Cooper, 2018). The transgression in the Mandawa Basin appears to be tectonically controlled. Early Cretaceous transtension and strike-slip faulting along E-W trending lineaments likely created localised accommodation space in the basin (Fossum et al., 2020).

The Nalwehe Sandstone Member is interpreted as marginal marine siliciclastic sediments deposited after a fall in sea-level. The measured section at locality MKW represents deposition in of fluvial derived sediments in a sag basin that developed in the Mbwemkuru area during the Early Cretaceous. In general, Late Jurassic and Early Cretaceous sandstones in the Mandawa Basin carry the same heavy mineral provenance signature. The sediments were derived from several different source terranes, mixed and homogenised during transportation and dispersed along the coast by waves and longshore currents (Fossum et al., 2018). A distinctly different provenance signature is observed in the MKW sandstones. The sand was derived mainly from amphibolite-facies rocks of the Masasi Basement Spur, showing minimal mixing with other sand sources (Fossum et al., 2018). The dominance of metamorphic rock fragments over sedimentary particles points to Early Cretaceous exhumation of the metamorphic basement to the west. The amphibole-bearing sandstones are restricted to Mbwemkuru area, which would suggest sediment transport by the Palaeo-Mbwemkuru River (Fossum et al., 2020).

During deposition of the Nalwehe Formation, large-scale tectonic readjustments occurred in the east. Seafloor spreading in the West Somali Basin ended, and relocated to the south to separate Antarctica and Madagascar/India, followed by strike-slip tectonics between Madagascar and India (Gaina et al., 2013; Tuck-Martin et al., 2017; Reeves, 2018). With the termination of seafloor spreading in the West Somali Basin, the Jurassic – Lower Cretaceous depositional cycle closed, and coastal Tanzania became part of a passive margin (Kent et al., 1971; Nicholas et al., 2006).

## 6. Concluding remarks and summary

The study of the Mandawa Basin geology is still in its infancy. The area north of the Matandu River is the least studied area, which is somewhat surprising since gas has been discovered in the Cretaceous Kipatimu Formation at SongoSongo. The onshore fluvial Kipatimu Formation sandstones provide good reservoirs with high porosities and

permeabilities. The WP92 section of the Kipatimu Formation is challenging and should be studied in more detail, as the stratigraphical development of the section has not yet been resolved and could provide important event information for correlation southwards within the basin. To this date biostratigraphic control is too poor for such correlations. The lower parts of the WP92 section bear lithological similarities to the dinosaur members of the Tendaguru Formation as described by Bussert et al. (2009).

The studied Upper Jurassic to Lower Cretaceous sections in the Mandawa Basin include fluvial sandstones (Kipatimu Formation), Kimmeridgian – Tithonian oncolitic limestones and shallow marine sandstones (Mitole Limestone Member), Tithonian tidal-channel and foreshore deposits (Mitole Sandstone Member), Lower Cretaceous lagoon and reef carbonates (Nalwehe Limestone Member) and marginal marine and estuarine sandstones (Nalwehe Sandstone Member and the Kipatimu Formation).

The results presented in this study are in overall agreement with previous interpretations of Late Jurassic – Early Cretaceous depositional environments in the Mandawa Basin, and can be summarised as follows:

- Sediment deposition occurred on a tidally influenced, mixed carbonate-siliciclastic ramp with cyclical transgressive-regressive sequences (limestones overlain by sandstones).
- Transgressive phases were characterised by microbial sedimentation and high rates of carbonate production, producing abundant micro-oncoids in the Late Jurassic and oncoids and stromatolites in the Early Cretaceous.
- High storm frequencies existed in the late Kimmeridgian – Tithonian times.
- A prolonged period of erosion and non-deposition presumably occurred in the Early Cretaceous.
- Early Cretaceous tectonism likely caused transgression in the basin by creating accommodation space.
- The depositional character of repetitive regressive-transgressive sedimentation ended when the passive margin along the East African coast was established in the Aptian.

## Declaration of competing interest

The authors declare that they have no known competing financial interests or personal relationships that could have appeared to influence the work reported in this paper.

## Acknowledgements

We wish to thank Equinor Tanzania for funding the Mandawa Basin Project. Sincere thanks to all who participated in the two field campaigns which includes students and staff from TDPC, the University of Dar es Salaam and UiO, and to Alexandra Cournot (Equinor). Thanks to Siri Simonsen, Maarten Aerts, Berit Løken Berg and Lars Riber at UiO for assisting with various analyses. The contribution from Nils Martin Hanken during microfacies analysis of carbonate rocks was highly appreciated. Thanks to Adrian Read, Nils Marin Hanken and to Pamela Sansom for improving earlier versions of this manuscript.

## Appendix A. Supplementary data

Supplementary data to this article can be found online at https://doi.org/10.1016/j.jafrearsci.2020.104013.

## References

Abbink, O.A., Van Konijnenburg-Van Cittert, J.H.A., Visscher, H., 2004. A sporomorph ecogroup model for the Northwest European Jurassic-Lower Cretaceous: concepts and framework. Neth. J. Geosci. 83, 17–31.

Aberhan, M., Bussert, R., Heinrich, W.-D., Schrank, E., Schultka, S., Sames, B., Kriwet, J., Kapilima, S., 2002. Palaeoecology and depositional environments of the Tendaguru beds (late jurassic to early cretaceous, Tanzania). Mitt Mus. Natur. Berl. 5, 17–44. Geowissenschaftliche Reihe.

Aitken, W.G., 1955. Notes on the makangaga-ruawa anticline. Kilwa Distr. Rec. Geol. Surv. Tanganyika III, 5–17. Government printer, Dar es Salaam, Tanzania.

Aitken, W.G., 1956. Further notes on the mandawa-mahokondo anticline. Kilwa Distr. Rec. Geol. Surv. Tanganyika III, 8–16. Government printer, Dar es Salaam, Tanzania.

Aitken, W.G., 1961. Geology and palaeontology of the jurassic and cretaceous of southern tanganyika. Bull. Geol. Surv. Tanganyika 31, 1–144. Government printer, Dar es Salaam, Tanzania.

Arkell, W.J., 1956. Jurassic Geology of the World. Oliver and Boyd Ltd, Edinburgh, UK, 806 pp.

Bádenas, B., Aurell, M., 2010. Facies models of a shallow-water carbonate ramp based on distribution of non-skeletal grains (Kimmeridgian, Spain). Facies 56, 89–110.

Balduzzi, A., Msaky, E., Trincianti, E., Manum, S.B., 1992. Mesozoic Karoo and post-Karoo Formations in the Kilwa area, southeastern Tanzania – a stratigraphic study based on palynology, micropalaeontology and well log data from the Kizimbai Well. J. Afr. Earth Sci. 15, 405–427.

Berner, R.A., 1984. Sedimentary pyrite formation: an update. Geochem. Cosmochemica Acta 48, 605–615.

Browne, K.M., Golubic, S., Seong-Joo, L., Riding, R.E., 2000. Shallow marine microbial carbonate deposits. In: Awramik, M. (Ed.), Microbial Sediments (. Springer-Verlag Berlin Heidelberg, pp. 233–249.

Bussert, R., Aberhan, M., 2004. Storms and tsunamis: evidence of event sedimentation in the Late Jurassic Tendaguru Beds of southeastern Tanzania. J. Afr. Earth Sci. 39, 549–555.

Bussert, R., Heinrich, W.D., Aberhan, M., 2009. The Tendaguru Formation (late jurassic to early cretaceous, southern Tanzania): definition, palaeoenvironments, and sequence stratigraphy. Foss. Rec. 12, 141–174.

Cant, D.J., Walker, R.G., 1978. Fluvial processes and facies sequences in the sandy braided South Saskatchewan River, Canada. Sedimentology 25, 625–648.

Clifton, H.E., Hunter, R.E., Phillips, R.L., 1971. Depositional structures and processes in the non-barred high-energy nearshore. J. Sediment. Petrol. 41, 651–670.

Collinson, J.D., 1970. Bedforms of the tana river, Norway. Geogr. Ann. Phys. Geogr. 52, 31–56.

Cooper, J.A.G., 2002. The role of extreme floods in estuary-coastal behaviour: contrasts between river- and tide-dominated microtidal estuaries. Sediment. Geol. 150, 123–137.

Cooper, M.R., 2018. Cretaceous Fossils of South-Central Africa: an Illustrated Guide. CRC Press, 164 pp.

Dahanayake, K., 1983. Depositional environments for some Upper Jurassic oncoids. In: Peryt, T.M. (Ed.), Coated Grains. Springer-Verlag Berling Heidelberg, Germany, pp. 377–385.

Davies Jr., R.A., 2012. Tidal signatures and their preservation potential in stratigraphic sequences. In: Davies, R.A., Dalrymple, R.W. (Eds.), Principles of Tidal Sedimentology. Springer Science and Buisness Medis, Dordrecht, Netherlands, pp. 35–56.

Didas, M.M., 2016. Geophysical Investigation of the Subsurface Structures of the Mandawa Basin, Southeast Coastal Tanzania. M.Sc. thesis, University of Dar es Salaam. 155 pp.

Doebelin, N., Kleeberg, R., 2015. Profex: a graphical user interface for the Rietveld refinement program BGMN. J. Appl. Crystallogr. 48, 1573–1580.

Dumas, S., Arnott, R.W.C., 2006. Origin of hummocky and swaley cross-stratification–the controlling influence of unidirectional current strength and aggradation rate. Geology 34, 1073–1076.

Dunham, R.J., 1962. Classification of carbonate rocks according to depositional textures. In: Ham, W.E. (Ed.), Classification of Carbonate Rocks: American Association of Petroleum Geologist Memoir 1, pp. 108–121.

Flügel, E., 2004. Microfacies of Carbonate Rocks. Analysis, Interpretation and Application, vol. 2. Springer-Verlag Berlin Heidelberg, 976pp.

Fossum, K., 2020. Jurassic – Cretaceous Stratigraphic Development of the Mandawa Basin, Tanzania: an Integrated Sedimentological and Heavy Mineral Study of the Early Post-rift Succession. Phd thesis, University of Oslo. 224 pp..

Fossum, K., Morton, A.C., Dypvik, H., Hudson, W.E., 2018. Integrated heavy mineral study of Jurassic to Paleogene sandstones in the Mandawa Basin, Tanzania: sediment provenance and source-to-sink relations. J. Afr. Earth Sci. 150, 546–565.

Fossum, K., Dypvik, H., Morton, A.C., 2020. Provenance studies of southern Tanzania river sediments: heavy mineral signatures and U-Pb zircon ages. J. Afr. Earth Sci. 170.

Frey, R.W., Goldring, R., 1992. Marine event beds and recolonization surfaces as revealed by trace fossil analysis. Geol. Mag. 129, 325–335.

Freytet, P., Verrencchia, E.P., 2002. Lacustrine and palustrine carbonate petrography: an overview. J. Paleolimnol. 27, 221–237.

Gaina, C., Torsvik, T.H., van Hinsbergen, D.J., Medvedev, S., Werner, S.C., Labails, C., 2013. The African Plate: a history of oceanic crust accretion and subduction since the Jurassic. Tectonophysics 604, 4–25.

Geiger, M., Clark, D.N., Mette, W., 2004. Reappraisal of the timing of the break-up of Gondwana based on sedimentological and seismic evidence from the Morondava Basin, SW Madagascar. J. Afr. Earth Sci. 338, 363–381.

Gundersveen, E., 2014. Sedimentology, Petrology and Diagenesis of Mesozoic Sandstones in the Mandawa Basin, Coastal Tanzania. M.Sc. thesis, Department of Geosciences, University of Oslo: 105 pp.

Hancox, P., Brandt, D., Edwards, H., 2002. Sequence stratigraphic analysis of the early cretaceous maconde formation (rovuma basin), northern Mozambique. J. Afr. Earth Sci. 34, 291–297.

Hennig, E., 1914. Beiträge zur Geologie und Stratigraphie Deutsch-Ostafrikas. Arch. Biontologie 1–72.

Hudson, W.E., 2011. The Geological Evolution of the Petroleum Prospective Mandawa Basin Southern Coastal Tanzania. Unpublished PhD Thesis, Trinity College, University of Dublin, Ireland: 357 pp.
Kent, P.E., Hunt, J.A., Johnstone, D.W., 1971. The Geology and Geophysics of Coastal Tanzania. Natural Environment Research Council, Institute of Geological Sciences. Geophysical paper 6: 101pp.
Krumbein, W.E. Stromatolites – the challenge of a term in space and time. Precambrian Res. 20: 493–531.
Leinfelder, R.R., Nose, M., Schmid, D.U., Werner, W., 1993. Composition, palaeoecological significance and importance in reef construction. Facies 29, 195–229.
Mahanjane, E.S., 2014. The Davie Fracture Zone and adjacent basins in the offshore Mozambique Margin – new insights for the hydrocarbon potential. Mar. Petrol. Geol. 57, 561–571.
Miall, A.D., 1977. A Review of the braided-river depositional environment. Earth Sci. Rev. 13, 1–62.
Mkuu, D.E., 2018. Palynological, Palynofacies, Thermal Maturity and Burial Modelling Analyses of the Cretaceous to Cenozoic Sediments from a Series of Tanzanian Onshore and Offshore Boreholes. Ph.D. thesis, University of Southampton, UK: 286 pp.
Mpanda, S., 1997. Geological Development of the East African Coastal Basin of Tanzania. PhD thesis. Department of Geology and Geochemistry, Stockholm University, Sweden: 121 pp.
Mpanju, F., Philp, R.P., 1994. Organic geochemical characterization of bitumen, seeps, rock extracts and condensates from Tanzania. Org. Geochem. 21, 359–371.
Msaky, E.S., 2007. Occurrence of dinoflagelate cyst genera *Wanaea* and *Komewuia* in Upper Jurassic strata, coastal Tanzania. Paleontol. Res. 11, 41–58.
Nerbråten, K.B., 2014. Petrology and Sedimentary Provenance of Mesozoic and Cenozoic Sequences in the Mandawa Basin. M.Sc. thesis, Department of Geosciences, University of Oslo: 114 pp.
Nicholas, C.J., Pearson, P.N., Bown, P.R., Jones, T.D., Huber, B.T., Karega, A., Lees, J.A., McMillan, I.K., O'Halloran, A., Singano, J.M., Wade, B.S., 2006. Stratigraphy and sedimentology of the upper cretaceous to paleogene Kilwa group, southern coastal Tanzania. J. Afr. Earth Sci. 45, 431–466.
Pemberton, S.G., Frey, R.W., 1984. Ichnology of storm-influenced shallow marine sequence: cardium formation (upper cretaceous) at seebe, alberta. In: Stott, D.F., Glass, D.J. (Eds.), The Mesozoic of Middle North America. Canadian Society Petroleum Geologists. Memoir 9: 281–304.
Pemberton, S.G., MacEachern, J.A., 1995. The sequence stratigraphic significance of trace fossils: examples from the Cretaceous foreland basin of Alberta, Canada. In: Van Wagoner, J.C., Bertram, G.T.( (Eds.), Sequence Stratigraphy of Foreland Basin Deposits. AAPG: 429–475.
Pemberton, S.G., MacEachern, J.A., Dashtgard, S.E., Bann, K.L., Gingras, M.K., Zonneveld, J., 2012. Shorefaces. In: Knaust, E., Bromly, R.G. (Eds.), Trace Fossils as Indicators of Sedimentary Environments. Developments in Sedimentology, vol. 64. Elsevier, pp. 563–603.
Peryt, T.M., 1981. Phanerozoic oncoids – an overview. Facies 4, 197–214.
Peryt, T.M., 1983. Oncoids: comment to recent developments. In: Peryt, T.M. (Ed.), Coated Grains. Springer-Verlag Berlin Heidelberg, Germany, p. 275.
Quennel, A.M., McKinlay, A.C.M., Aitken, W.G., 1956. Summary of the geology of Tanganyika; Part 1. Introduction and stratigraphy, 1. Geological Survey of Tanganyika Memoir. Dar es Salaam: 264pp.
Reeves, C.V., 2018. The development of the East African margin during Jurassic and Lower Cretaceous times: a perspective from global tectonics. Petrol. Geosci. 24, 41–56.
Reineck, H.-E., Wunderlich, F., 1968. Classification and origin of flaser and lenticular bedding. Sedimentology 11, 99–104.
Reolid, M., Gaillard, C., 2007. Microtaphonomy of bioclasts and paleoecology if microencrusters from upper jurassic spongiolithic limestones (external prebetic, southern Spain). Facies 56, 97–112.
Reolid, M., Gaillard, C., Olóriz, F., Rodríguez-Tovar, F.J., 2005. Microbial encrustations from the middle oxfordian-earliest kimmeridgian lithofacies in the prebetic zone (betic cordillera, southern Spain): characterization, distribution and controlling factors. Facies 50, 529–543.
Richter, D.K., 1983. Calcareous ooids: a synopsis. In: Peryt, T.M. (Ed.), Coated Grains. Springer-Verlag Berling Heidelberg, Germany, pp. 71–99.
Rust, B.R., 1972. Structure and process in a braided river. Sedimentology 18, 221–245.
Sansom, P., 2016. Sequence stratigraphic scheme for the Jurassic-Neogene of coastal and offshore Tanzania. Res. Reserv. 1, 33–37.
Sansom, P., 2018. Hybrid turbidite–contourite systems of the Tanzanian margin. Petrol. Geosci. 24, 258–276.
Smelror, M., Key, R.M., Smith, R.A., Njange, F., 2008. Late jurassic and cretaceous palynostratigraphy of the onshore rovuma basin, northern Mozambique. Palynology 32, 63–76.
Smelror, M., Fossum, K., Dypvik, H., Hudson, W.E., Mweneinda, A., 2018. Late jurassic – early cretaceous palynostatigraphy of the onshore Mandawa Basin, southeastern Tanzania. Rev. Palaeobot. Palynol. 258, 248–255.
Smith, N.D., 1972. Some sedimentological aspects of planar cross-stratification in a sandy braided river. J. Sediment. Res. 42, 625–634.
Stear, W.M., 1985. Comparison of the beform distribution and dynamics of modern and ancient sandy ephemeral flood deposits in the southwestern Karoo region, South Africa. Sediment. Geol. 45, 209–230.
Stockley, G.M., 1935. A further contribution on the Karroo rocks of Tanganyika Territory. Q. J. Geol. Soc. Lond. 92, 1–30.
Stockley, G.M., 1943. The geology of the Rufiji district, including a small portion of the northern Kilwa district, (matumbi hills). Tanzan. Notes Rec. 16, 7–28.
Stolz, J.F., Riding, R.E., 2000. Structure of microbial mats and biofilms. In: Awramik, M. (Ed.), Microbial Sediments. Springer-Verlag Berlin Heidelberg, pp. 1–8.
Tuck-Martin, A., Adam, J., Eagles, G., 2018. New plate kinematic model and tectono-stratigraphic history of the east african and West madagascan margins. Basin Res. 30, 1118–1140.
Van den Brink, M., 2015. Depositional Environments and Mineralogical Characterization of the Upper Jurassic Mitole Formation, Southern Coastal Tanzania. M.Sc. thesis, Department of Geosciences, University of Oslo: 87 pp.
Védrine, S., Strasser, A., Hug, W., 2007. Oncoid growth and distribution controlled by sea-level fluctuations and climate (Late Oxfordian, Swiss Jura Mountains). Facies 53, 535–552.
Visser, M.J., 1980. Neap-spring cycles reflected in Holocene subtidal large-scale bedform deposits: a preliminary note. Geology 8, 543–546.
Wang, P., 2012. Principles of sediment transport applicable in tidal environments. In: Davies, R.A., Dalrymple, R.W.( (Eds.), Principles of Tidal Sedimentology. Springer Science and Buisness Medis, Dordrecht, Netherlands, pp. 19–34.
Wright, V.P., 1982. The recognition and interpretation of paleokarsts: two examples from the Lower Carboniferous of south Wales. J. Sediment. Petrol. 52, 83–94.
Wright, V.P., 1983. Morphogenesis of oncoids in the lower carboniferous llannely formation of south wales. In: Peryt, T.M. (Ed.), Coated Grains. Springer-Verlag Berling Heidelberg, Germany, pp. 424–434.